Lawrence Berkeley National Laboratory
LBL Publications

Title
Constraining GREA, an alternative theory accounting for the present cosmic acceleration

Permalink
https://escholarship.org/uc/item/9409j032

Journal
Journal of Cosmology and Astroparticle Physics, 2026(09)

ISSN
1475-7516

Authors
Calderon, R
García-Bellido, J
Vos-Ginés, B
et al.

Publication Date
2026-09-01

DOI
10.1088/1475-7516/2026/09/080

Copyright Information
This work is made available under the terms of a Creative Commons Attribution License, available at https://creativecommons.org/licenses/by/4.0/

Peer reviewed

eScholarship.org Powered by the California Digital Library
University of California

Journal of Cosmology
and Astroparticle
Physics

SISSA

PAPER • OPEN ACCESS

Constraining GREA, an alternative theory accounting for the present cosmic acceleration

To cite this article: R. Calderon *et al* JCAP09(2026)080

View the article online for updates and enhancements.

You may also like

- Measuring Dark Energy with Gamma-Ray Bursts and Other Cosmological Probes
F. Y. Wang, Z. G. Dai and Zong-Hong Zhu
- Cascading Dark Energy
Kazem Rezazadeh, Amjad Ashoorioon and Daniel Grin
- The Pantheon+ Analysis: Cosmological Constraints
Dillon Brout, Dan Scolnic, Brodie Popovic et al.

This content was downloaded from IP address 108.75.79.166 on 03/11/2026 at 21:33

Journal of Cosmology and Astroparticle Physics
An IOP and SISSA journal

Received: *March 2, 2026*
Accepted: *July 21, 2026*
Published: *September 16, 2026*

Constraining GREA, an alternative theory accounting for the present cosmic acceleration

R. Calderon, J. García-Bellido et al.
Full author list at the end of the paper

E-mail: calderon@fzu.cz, juan.garciabellido@uam.es

Abstract: The origin of the Universe's late-time accelerated expansion remains unknown. The General Relativistic Entropic Acceleration (GREA) theory offers a compelling alternative to ΛCDM, attributing cosmic acceleration to entropy growth associated with cosmic and black hole horizons, without invoking a cosmological constant. We test GREA against the latest DESI DR2 Baryon Acoustic Oscillations (BAO), multiple Type Ia supernova compilations (Union3, Pantheon+, DES-SN5YR), and cosmic microwave background (CMB) distance measurements. While GREA is not nested within ΛCDM, it achieves a comparable goodness-of-fit, highlighting its potential as a theoretically motivated framework that circumvents some of the fine-tuning issues of the standard ΛCDM cosmology. We find that the best-fit model features a transient phantom crossing at $z \lesssim 2$, with $w_a \equiv \mathrm{d}w(a=1)/\mathrm{d}a \simeq -0.3$, in good agreement with observations. However, its present-day value $w_0 \equiv w(z=0)$ is tightly constrained to be $w_0 \simeq -1$. Upcoming low-redshift (i.e. $z < 1$) cosmological probes, from both background and perturbations, will offer promising avenues for further exploring the viability of the GREA theory.

Keywords: dark energy theory, gravity, galaxy clustering, supernova type Ia - standard candles

ArXiv ePrint: 2509.21491

© 2026 The Author(s). Published by IOP Publishing Ltd on behalf of Sissa Medialab. Original content from this work may be used under the terms of the Creative Commons Attribution 4.0 licence. Any further distribution of this work must maintain attribution to the author(s) and the title of the work, journal citation and DOI.

https://doi.org/10.1088/1475-7516/2026/09/080

JCAP09(2026)080

Contents

1 Introduction **1**

2 Theoretical background **3**

3 Datasets **4**

4 Methodology **6**

5 Results and discussions **7**
- 5.1 Late-time probes 7
- 5.2 The role of the CMB 8
- 5.3 Implications for the Hubble tension 12
- 5.4 Further constraining GREA 14

6 Conclusions **15**

A Parameter constraints **18**

B Comparison with DESI DR1 **18**

C CMB compression and comparison with CamSpec PR4 **20**

D Impact of the DES Y5 Dovekie reanalysis **21**

Author List **28**

JCAP09(2026)080

1 Introduction

The cause of the Universe's accelerated expansion remains unknown. For the past two decades, the standard cosmological model (ΛCDM) has explained it through a cosmological constant, Λ [1]. While this model has been in remarkable agreement with a broad range of observations [2–6], it faces serious theoretical challenges, such as the fine-tuning and coincidence problems [7, 8], and lacks a fundamental explanation for its two main components: dark energy and dark matter. In addition, growing observational tensions and anomalies [9–13]—including discrepancies in the inferred values of the Hubble constant [14–16] and the amplitude of matter fluctuations[1] [18–21]—have raised questions about the validity of ΛCDM. More recently, data from the Dark Energy Spectroscopic Instrument (DESI), combined with other cosmological probes, have added to this picture by hinting at $\sim 4\sigma$ deviations from a ΛCDM expansion history [22, 23]. If confirmed, these results could represent the first evidence for new physics beyond ΛCDM. While they are often interpreted as signs of a dynamical dark

[1] Although the latest results from the KiDS legacy are fully compatible with the inferred values from the CMB [17].

energy component [22–28], alternative explanations have been proposed, including exotic neutrino masses [29, 30] or non-standard dark matter evolution [31, 32], among others [33–38].

Common approaches for modeling dark energy often rely on arbitrary parametrizations of the equation of state parameter, $w(z) = P/\rho$, or non-parametric reconstruction techniques [39–44], which provide limited physical insight. Parametric models, such as w_0w_aCDM [45, 46], are widely used due to their simplicity and connection with known physics [26, 46–48]. However, they risk biasing the inference if the true $w(z)$ deviates significantly from the assumed (parametric) form. Non-parametric methods offer greater flexibility, but require careful validation and can be difficult to interpret physically. A more informative strategy is to explore models grounded in theoretical principles. In this work, we investigate General Relativistic Entropic Acceleration (GREA) [49], a theory in which cosmic acceleration arises from the entropy growth associated with cosmological horizons [50]. GREA offers a novel, conceptually motivated alternative to ΛCDM and allows for direct connections between cosmology and fundamental physics. In the cosmological context, the GREA theory predicts that the present acceleration of the universe could arise from the growth of entropy associated with cosmic [49] and black hole horizons [51], without the need to introduce a cosmological constant, providing an alternative dynamics to that of ΛCDM. The GREA theory gives a covariant formalism for out of equilibrium dynamics in the context of general relativity. A consequence of GREA is the explicit breaking of the time reversal invariance when there is entropy production. This drives an entropic force that behaves effectively like bulk viscosity with a negative effective pressure [51].

Already before the recent evidence of significant deviations from the standard model of cosmology through state-of-the-art observations by DES-Y5 SNe [52] and DESI [22–24, 26, 27, 53], GREA was found to provide an equally good description of cosmological observations than ΛCDM [54]. Furthermore, GREA not only explains the coincidence problem, but can also help ease the Hubble tension by shifting the coasting point (when the universe transitioned from matter domination to acceleration) to higher redshifts and extending the period of acceleration [55]. In a recent paper [55], we performed a detailed calculation of the background and linear matter perturbations with the assumption that the entropy growth responsible for the accelerated expansion comes from the homogeneous cosmological horizon. We could show that, in this case, the dynamics can be described in terms of just one parameter, α, the ratio of the spatial curvature to the horizon distance. A given value of α defines a unique expansion history of the universe, with a dynamics that differs from ΛCDM and gives an explicit prediction for all background observables, like the values of the matter and dark energy content of the universe, the rate of expansion today, the coasting point, the value of the equation of state of dark energy and its derivative, the angular diameter and luminosity distances, etc. In this work, we use different observational datasets, including the latest baryon acoustic oscillation (BAO) measurements from DESI, to constrain the expansion history, as predicted by GREA.

This paper is structured as follows. In section 2, we introduce the theoretical background and details of GREA. We describe the observational datasets in section 3, and the methodology used in the analysis in section 4. Finally, we present our results in section 5 and conclude

JCAP09(2026)080

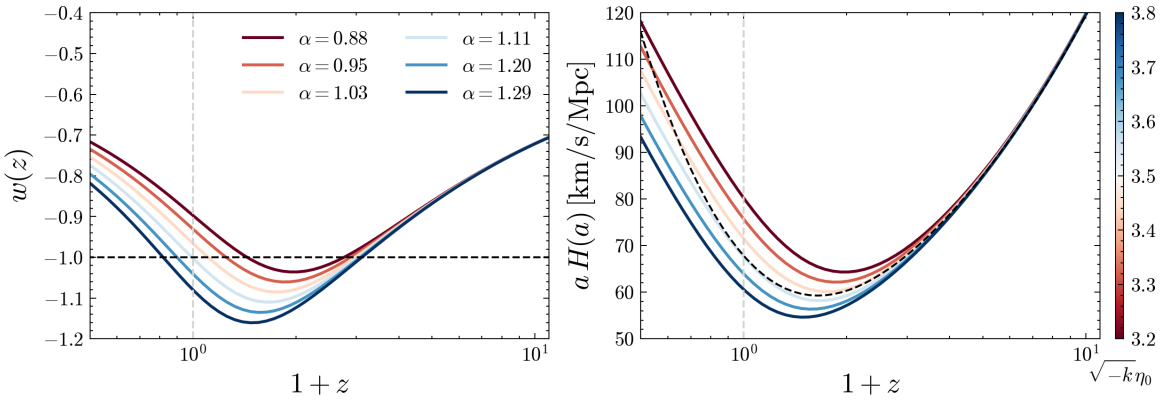


Figure 1. *Left:* the equation of state in GREA, for various values of the parameter α (or, equivalently $\sqrt{-k}\,\eta_0$), as obtained by integrating eq. (2.1) with initial (CMB-asymptotic) $\Omega_m = 0.31, h = 0.678$. Note that for some parameter combinations, the *effective* w in GREA features a (transient) phantom crossing—without violating the NEC—and generically predicts a slope of $w_a \simeq -0.3$, in line with observations *Right:* $\dot{a} \equiv aH(a)$ as a function of redshift. The dashed black lines in both figures correspond to ΛCDM.

in section 6. A quantitative comparison of the Hubble tension across all models considered in this work is provided in section 5.3.

2 Theoretical background

To obtain the expansion history of the Universe in GREA, we numerically solve for the (rescaled) conformal time $\tau \equiv H_0\eta = H_0 \int \frac{dt}{a(t)}$, using

$$\tau' \equiv \frac{d\tau}{da} = \left[a^2 \sqrt{\Omega_{\mathrm{m},0} a^{-3} \left(1 + \frac{a_{\mathrm{eq}}}{a}\right) + \frac{4\pi}{3a^2} \frac{\sinh(2\tau)}{(-k)^{3/2} V_c}} \right]^{-1} , \tag{2.1}$$

where $a_{\mathrm{eq}} \equiv \Omega_{\mathrm{r},0}/\Omega_{\mathrm{m},0}$ is the scale factor at matter-radiation equality, and where $\Omega_{r,0} = \Omega_{\gamma,0} + \Omega_{\nu,0}$ accounts for photons and (massless) neutrinos and $\Omega_{\mathrm{m},0} = \Omega_{\mathrm{b},0} + \Omega_{\mathrm{cdm},0}$ for baryons and cold dark matter, respectively. In this framework, it is possible to show (see [55]) that the comoving volume, V_c, is related to the spatial curvature, k, and the conformal time $\eta_0 = \eta(z = 0)$ by

$$(-k)^{3/2} V_c = \pi \left[\sinh\left(2\sqrt{-k}\,\eta_0\right) - 2\sqrt{-k}\,\eta_0 \right] . \tag{2.2}$$

It is the second term in eq. (2.1) that plays the role of the dark energy, and drives the late-time accelerated expansion of the Universe. The phenomenology of GREA can be characterized with a single $\mathcal{O}(1)$ parameter, α, defined as [55]

$$\alpha\, \mathcal{D}_H(z = 0) = \sqrt{-k}\,\eta_0 \,, \tag{2.3}$$

where $\mathcal{D}_H(a) \equiv H(a)\, d_H(a) = Ha\,\eta(a)$ is the *dimensionless* horizon distance, computed from eq. (2.1).[2] Its value today is $\mathcal{D}_H(z = 0) \neq \tau_0$. As is clear from eq. (2.3), α determines the size

[2] In wCDM, this is given by $\mathcal{D}_H(a) = \frac{2}{\sqrt{\Omega_m}} a^{3/2} \cdot {}_2F_1\left[\frac{1}{2}, \frac{-1}{6w}, 1 - \frac{1}{6w}, \frac{\Omega_m - 1}{\Omega_m} a^{-3w}\right]$.

JCAP09(2026)080

of the curvature scale, $\sqrt{-k}\eta_0$, relative to the causal horizon today. We integrate eq. (2.1) with initial conditions deep in the radiation era $\tau(a_{\rm ini} = 10^{-11}) = a_{\rm ini}/\sqrt{\Omega_\gamma + \Omega_\nu}$, giving $\tau(a)$. The effect of varying α on the *effective* equation of state component, $w \equiv P/\rho$, and expansion history is shown in figure 1, where the corresponding values for $\sqrt{-k}\,\eta_0$ are reported in the color bar, and where the black dashed line depicts the ΛCDM predictions.

3 Datasets

To derive cosmological constraints on GREA, we use the most recent Baryon Acoustic Oscillations (BAO) observations from the Dark Energy Spectroscopic Instrument (DESI) [24] along with different supernovae Ia (SNe Ia) compilations and cosmic microwave background (CMB) data. Here we briefly explain the data and methods we use in this analysis.

Our main observational data set is the baseline Baryon Acoustic Oscillations (BAO) data (DR2) from the Dark Energy Spectroscopic Instrument (DESI) [22, 24, 26, 56]. We combine the DESI DR2 BAO data with complementary data sets: Supernovae Ia, Cosmic Microwave Background and Big-Bang Nucleosynthesis, as described below.

Baryon Acoustic Oscillations (BAO). This dataset, abbreviated as "DESI BAO", spans seven redshift bins from $z = 0.3$ to $z = 2.33$ (where the last bin extends out to $z \approx 3.5$) [57]. DESI is an optical spectroscopic Stage IV survey carrying out a 3-D map over 14,000 square degrees and within the redshift range $0.1 < z < 4.2$ [58–66]. DESI was designed to improve cosmological constraints on both the expansion history and the growth rate of large scale structure, through measurements of the clustering of galaxies (BGS, LRGs and ELGs), quasars or QSOs, and the Lyman-α forest [67–70]. In this work, we use the BAO measurements from the first 3 years of DESI observations [71]. The galaxy and quasar BAO measurements used here are in configuration space [57].

Transverse to the line of sight, DESI constrains the ratio between the comoving angular diameter distance, D_M, at the effective redshift of the galaxy sample, $z_{\rm eff}$, and the sound horizon at drag time, $r_d \equiv r_s(z_{\rm drag})$, [57]:

$$\frac{D_M(z_{\rm eff})}{r_{\rm d}} \equiv \frac{c}{r_{\rm d}} \int_0^{z_{\rm eff}} \frac{dz'}{H(z')} = \frac{c}{H_0 r_{\rm d}} \int_0^{z_{\rm eff}} \frac{dz'}{E(z')}\,, \tag{3.1}$$

[3] where c is the speed of light and $E(z) = H(z)/H_0$ is the normalized Hubble rate. The radial measurements of the BAO constrain the ratio between the Hubble distance $D_H \equiv c/H(z)$, at the effective redshift of the galaxy sample, $z_{\rm eff}$, and the sound horizon at drag epoch, r_d:

$$\frac{D_H(z_{\rm eff})}{r_{\rm d}} \equiv \frac{c}{H(z_{\rm eff}) r_{\rm d}} = \frac{c}{H_0 r_{\rm d}} \frac{1}{E(z_{\rm eff})}\,. \tag{3.2}$$

[3] In GREA, derived in the context of open inflation [55], our observable universe is a spatially flat bubble ($\Omega_K = 0$) nucleated inside a larger hyperbolic space. The parameter k (equivalently $\kappa = \sqrt{-k}\,\eta_0$) characterises the *size* of the causal boundary rather than the spatial curvature of the local metric; it enters the dark energy source through the comoving horizon volume $(-k)^{3/2} V_c = \pi[\sinh(2\kappa) - 2\kappa]$ but does not curve the spatial sections that photons traverse. The flat expression $D_M = c\int_0^z dz'/H(z')$ is therefore exact within the GREA framework.

JCAP09(2026)080

In the equations above, eqs. (3.1) and (3.2), we explicitly factored out the absolute scaling set by the (degenerate) combination $H_0 r_{\rm d}$. For the lowest redshift bin, corresponding to the BGS sample, we use the volume-averaged quantity:

$$\frac{D_V(z_{\rm eff})}{r_{\rm d}} \equiv [z_{\rm eff} D_M^2(z_{\rm eff}) D_H(z_{\rm eff})]^{1/3}/r_{\rm d}\,. \tag{3.3}$$

One crucial quantity for the analysis is the sound horizon, r_s, defined as

$$r_s(z) = \int_z^\infty \frac{c_s(z')}{H(z')} dz'\,, \tag{3.4}$$

where $c_s(z)$ is the sound speed of the photon-baryon plasma, given by

$$c_s^2(z) = \frac{c^2}{3(1+\frac{3}{4}R(z))}\,, \quad R(z) \equiv \frac{\rho_b(z)}{\rho_\gamma(z)}\,, \tag{3.5}$$

and c denotes the speed of light in vacuum. The sound horizon in eq. (3.4) is evaluated at the baryon drag epoch $z_{\rm drag} \simeq 1066$, and at recombination $z_* \simeq 1089$. The exact values for $z_{\rm drag}$ and z_* are obtained using the approximations presented in [72]. These approximations provide subpercent accuracy for a wide range of parameter values, and they are further justified by the fact that at high-redshifts, GREA has a ΛCDM-like expansion history. This is shown in the right panel of figure 1.

Supernovae Ia (SNe Ia). We use supernova (SN) data from three sets: "Pantheon+", "Union3", and "DES-SN5YR". "Pantheon+" is a compilation of 1550 supernovae spanning the redshift range $0.01 < z < 2.26$ [73]. "Union3" contains 2087 SNe Ia processed through the Unity 1.5 pipeline based on Bayesian Hierarchical Modelling [74]. "DES-SN5YR" is a compilation of 194 low-redshift SNe Ia ($0.025 < z < 0.1$) and 1635 photometrically classified SNe Ia covering the range $0.1 < z < 1.3$ [52]. These constrain the distance modulus

$$\mu(z) = m_B(z) - M_B = 5\log_{10}(D_L(z)/{\rm Mpc}) + 25\,, \tag{3.6}$$

where $D_L(z) = (1+z)D_M(z)$ is the luminosity distance, encoding the cosmological model-dependence. $m_B(z)$ and M_B are the apparent and absolute magnitude, respectively. In this work, we treat M_B as a nuisance parameter.

SH0ES measurement of H_0. The Pantheon+ sample includes a set of very low-redshift Type Ia supernovae with Cepheid-based distance calibrations [14, 73]. These serve as the local anchor in the distance ladder and effectively constrain the Hubble constant, H_0, or equivalently, the absolute magnitude of Type Ia supernovae, M_B. In practice, we use the `pantheonplusshoes`[4] likelihood, as implemented in COBAYA , and refer to this as Pantheon+ & $\rm SH_0ES$.

Cosmic Microwave Background (CMB). Following [23, 71], we use the compressed CMB information in terms of $(\theta_s, \omega_{\rm b}, \omega_{\rm cb})$. These have been found to yield nearly identical constraints on late-time dark energy as the full CMB likelihood. The mean values and covariance matrix have been extracted from the publicly available[5] P-ACT ΛCDM chains [75, 76], and include both Planck PR4 [77] and ACT DR6 lensing [78, 79]).

[4] https://cobaya.readthedocs.io/en/latest/likelihood_sn.html.

[5] The chains can be found at https://act.princeton.edu/act-dr6-data-products.

JCAP09(2026)080

parameter	prior	model
$\omega_{\rm cdm} \equiv \Omega_{\rm cdm,0} h^2$	$\mathcal{U}[0.05, 0.5]$	All
$\omega_{\rm b} \equiv \Omega_{\rm b,0} h^2$	$\mathcal{U}[0.005, 0.1]$	All
H_0 $[\,{\rm km\,s^{-1}\,Mpc^{-1}}]$	$\mathcal{U}[20, 100]$	All
$\sqrt{-k}\eta_0$	$\mathcal{U}[1, 5]$	GREA
$\Omega_{\rm k,0}$	$\mathcal{U}[-0.3, 0.3]$	ΛCDM + $\Omega_{\rm k}$

Table 1. Parameters and priors used in the analysis. All of the priors are uniform in the ranges specified below, except for the runs including +BBN, where a Gaussian prior on ω_b is used instead [80]. The "Model" column specifies which model each parameter belongs to: parameters labeled "All" are common to every model considered in this work, while $\sqrt{-k}\eta_0$ is specific to GREA and $\Omega_{k,0}$ to ΛCDM+Ω_k; these are *not* simultaneously free parameters of any single model.

Big-Bang Nucleosynthesis (BBN). When we don't include the CMB data, we include a prior on $\omega_b \equiv \Omega_b h^2$ from big-bang nucleosynthesis (BBN) [80] to break the H_0-$r_{\rm d}$ degeneracy and "calibrate" the distances from BAO and SNe.

4 Methodology

To confront the predictions of GREA to the data, we numerically implement eq. (2.1) into a Python package, `greapy` . We then sample the posterior distribution of GREA using Markov Chain Monte Carlo (MCMC) methods. In particular, we use the Metropolis-Hastings algorithm [81, 82], as implemented in the publicly available sampler COBAYA [83]. The parameter space associated with GREA is $\Theta = \{H_0, \omega_{\rm cdm}, \omega_b, \sqrt{-k}\eta_0\}$ and unless specified otherwise, we assume flat uninformative priors on all parameters, listed in table 1. Throughout this work, we assume massless neutrinos, with $N_{\rm eff} = 3.044$ and a fixed spectral index, $n_s = 0.965$. We do not expect the inclusion of massive neutrinos or a different spectral tilt to significantly alter our conclusions, as none of the observables used in the analysis are sensitive to such parameters. We assess the convergence of our MCMC chains using the Gelman-Rubin $(R-1)$ criterion [84] and require all of our chains to satisfy $R - 1 < 0.01$. We analyze our chains and produce our plots using the python package `GetDist` [85]. Finally, for the Pantheon+, DES-SN5YR, and Union3 likelihoods, the marginalization over the absolute magnitude M_B is done analytically. As in previous DESI analyses, we adopt the $\alpha_\perp$ and $\alpha_\parallel$ parametrization to characterize the angular and radial BAO scales relative to a fiducial ΛCDM model. While a fully consistent treatment would involve recomputing the anisotropic two-point correlation function within the GREA framework, this is beyond the scope of the present work. Nonetheless, we note that the standard BAO compression scheme has been shown to be robust for a wide class of cosmological models, including those beyond ΛCDM [86]. In particular, GREA belongs to the class of homogeneous and isotropic FLRW models, and its linear perturbation theory yields a growth history (figure 10) that encompasses that of ΛCDM [55]. The primary difference lies in the dynamical evolution of the effective dark energy component.

JCAP09(2026)080

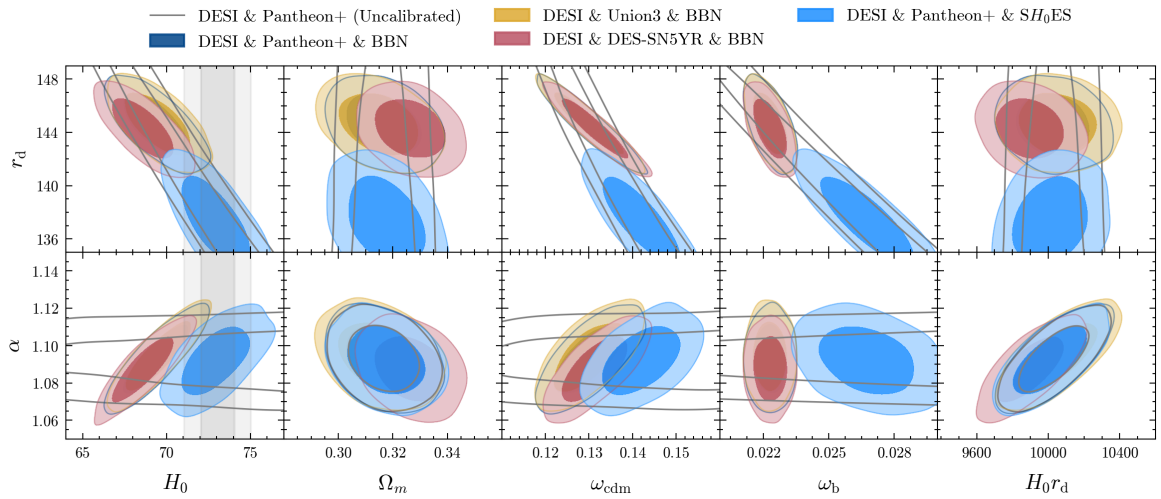


Figure 2. Marginalized constraints on parameters of GREA from DESI BAO DR2 and the various SNe Ia compilations: "Pantheon+", "Union3", and "DES-SN5YR" (section 3). We show the impact of an early-universe calibration of distances through the inclusion of a BBN-prior on $\omega_b \equiv \Omega_b h^2$ [80], or at late-times by including SH_0ES [14]. The light gray unfilled contours show the uncalibrated results when using the DESI BAO and Pantheon+ datasets, which constrain only the product $H_0 r_d$ and $\Omega_{m,0}$. For reference, we show here the H_0 measurements from SH_0ES [14] with the light grey vertical bands. The inferred parameters are consistent for the Pantheon+, Union3, and DES-SN5YR SN datasets.

To compute the Bayesian Evidence $\mathcal{Z}$ required for model selection, we use the nested-sampling algorithm implemented in POLYCHORD [87, 88] for specific data combinations. In essence, Bayesian Evidence enables the direct comparison of competing models via their ratio, known as the Bayes factor, K, which quantifies the relative support for one model over another by simultaneously considering the goodness of fit and penalizing for model complexity. However, it is important to note that model selection based on the Bayes factor has limitations, and conclusions drawn from such analyses must be interpreted with caution [89–91]. The interpretation of the Bayes factor can be sensitive to the choice of priors, not only parameter ranges but also theoretical priors, and its effectiveness may diminish when comparing models that differ significantly in their underlying theoretical assumptions or parameter space.

5 Results and discussions

5.1 Late-time probes

We begin by discussing the results obtained from late-time (low-redshift) probes. figure 2 presents the constraints derived from combining the DESI DR2 BAO measurements with various available supernova Ia (SNe Ia) compilations (section 3). The light gray (unfilled) contours represent the uncalibrated DESI BAO and Pantheon+ datasets, which constrain only the fractional matter density, $\Omega_{m,0}$, and the absolute scaling, $H_0 r_d$. The uncalibrated distances probed by the SN+BAO combination constitute a sensitive probe of the shape of the expansion history $E(z) \equiv H(z)/H_0$, as seen from eqs. (3.1), (3.2) and (3.6). Thus,

JCAP09(2026)080

the *uncalibrated* SN+BAO data alone can constrain the fractional matter density, $\Omega_{\rm m,0}$, and α, but not the individual physical densities $\omega_{\rm b}$ and $\omega_{\rm c}$.

The late-time probes (SN & BAO) allow for values of H_0 compatible with SH$_0$ES [14] (shown as a vertical shaded band in figure 2) while implying a reduced size of the sound horizon, relative to ΛCDM, and therefore an increase in $\omega_{\rm b}$ (in tension with BBN). Such a value of H_0, in combination with a large $\Omega_{\rm m,0}$, inevitably leads to an increase of $\omega_m = \omega_{\rm cdm} + \omega_{\rm b} = \Omega_{\rm m,0}h^2$ (figure 2). This is common to many models attempting to address the Hubble tension, as recently emphasized in [92, 93]. Such an increase in the physical matter density has important implications for the acoustic peaks in the cosmic microwave background and the clustering of matter at late times.

To break the H_0-$r_{\rm d}$ degeneracy, we also incorporate a big-bang nucleosynthesis (BBN) prior on $\omega_b = (2.231 \pm 0.05) \times 10^{-2}$ [80], effectively calibrating distances in the early universe by fixing the size of the standard ruler, $r_{\rm d}$. The constraints on $\alpha = 1.09 \pm 0.012$ are stable across different SN compilations, while the constraints on $\Omega_{\rm m,0}$ marginally depend on the choice of SN, with DES-SN5YR driving the preference for higher matter densities with respect to Pantheon+ and Union3, in agreement with previous findings [22, 24, 26, 52]. For conciseness, in what follows we will focus on and only show results using the Pantheon+ compilation.

5.2 The role of the CMB

In figure 3, we report the constraints including CMB information. The CMB constrains the late-time expansion history primarily through an exquisite ($\sim 0.04\%$) measurement of the acoustic scale $\theta_s \equiv r_s(z_*)/D_M(z_*)$. Recall that the relative height of odd/even acoustic peaks in the CMB tightly constrains the physical baryon density, $\omega_{\rm b} = \Omega_{\rm b,0}h^2$ [94, 95]. Thus, the angular size of the sound horizon, together with the physical energy densities $\omega_{\rm b}$ and $\omega_{\rm cdm}$, carries most of the geometrical information contained in the CMB. Within ΛCDM, the CMB distance priors provide constraints on the fractional matter density, $\Omega_{\rm m,0}$, and Hubble constant, H_0. In GREA, however, because of the degeneracies introduced by the parameter α, we can no longer estimate $\Omega_{\rm m,0}$ and H_0 purely from such measurements (as shown by the gray contours in figure 3). This is reminiscent of the intrinsic geometrical degeneracy between matter and dark energy ($\Omega_{\rm m,0}$ and $w(z)$) [e.g. 43, 96–99].

Let us now discuss the results of the DESI BAO & CMB combination. While the CMB is sensitive to the product $\Omega_{\rm m,0}h^2$, DESI BAO measurements probe the fractional matter density $\Omega_{\rm m,0}$ directly. Thus, including the DESI data breaks these degeneracies by providing constraints on $\Omega_{\rm m,0}$ (see figure 3). In turn, this allows for an estimation of H_0, and more importantly, of α, which characterizes the phenomenology of GREA. Including SNe Ia distance measurements, which are also highly sensitive to the fractional matter density, yield constraints of $\Omega_{\rm m,0} = 0.317 \pm 0.009$ ($\Omega_{\rm m,0} = 0.292 \pm 0.004$) for the DESI BAO & Pantheon+ & BBN (DESI BAO & Pantheon+ & CMB) combination. Notably, swapping Pantheon+ with the DES-SN5YR compilation pushes H_0 to lower values, due to the preference for a higher $\Omega_{\rm m,0}$ in comparison to Pantheon+. The derived constraints on the effective equation-of-state parameters w_0 and w_a are shown in figure 4.

These differences in $\Omega_{\rm m,0}$ between analyses with and without Pantheon+ are reflected in the degraded fit quality to the combined data, as shown in table 2. This fit degradation, driven

JCAP09(2026)080

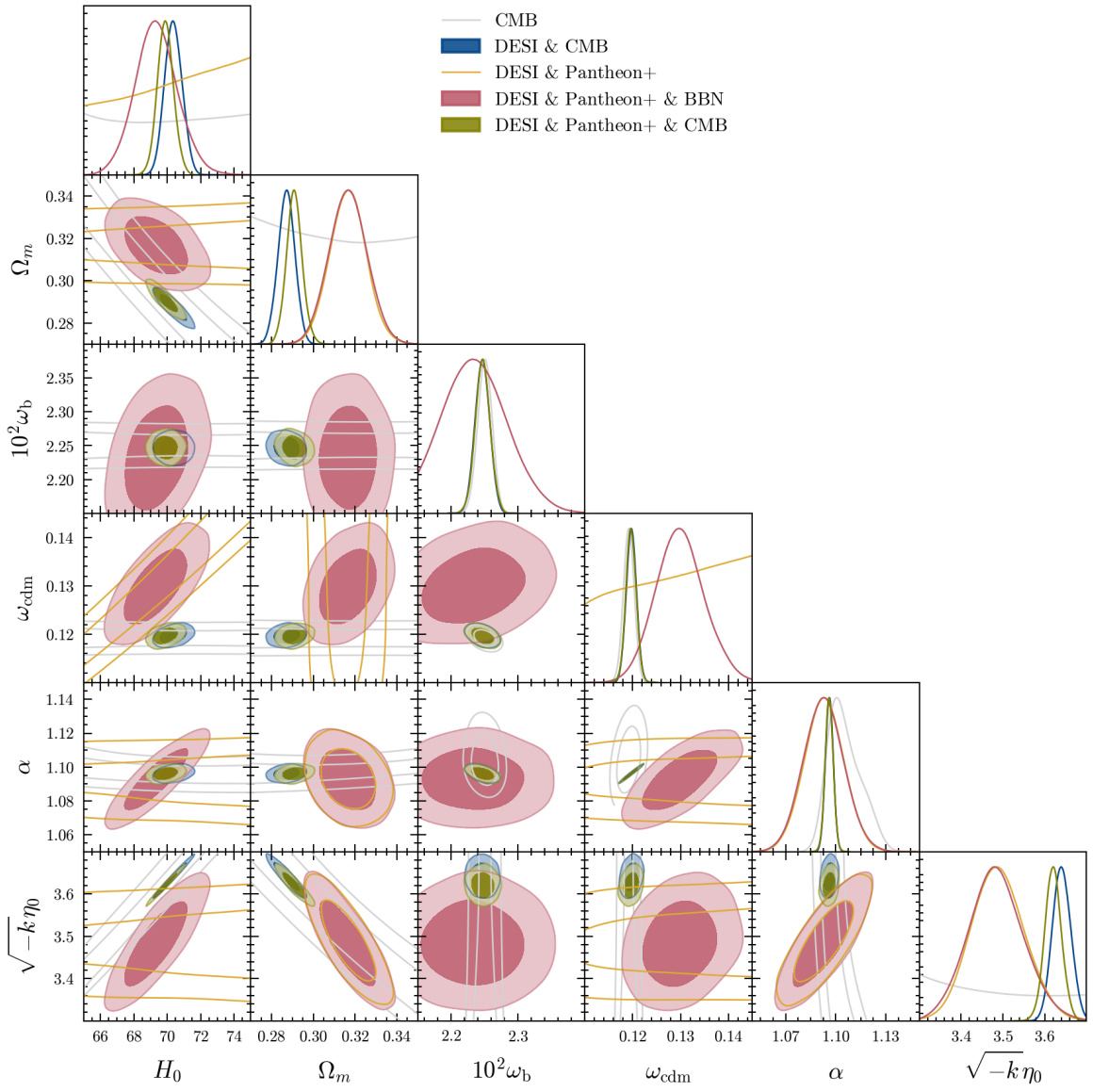


Figure 3. The full posterior distribution for GREA's cosmological parameters (section 2), inferred from fitting the model to different datasets, including DESI DR2 [71], as indicated in the legend. The light gray unfilled contours show the uncalibrated results when using the CMB data from P-ACT (section 3), which is sensitive to the product $\Omega_{m,0}h^2$. Note that the Pantheon+ data prefer higher matter densities than the DESI & CMB datasets, leading to some tension in some of the projected parameter space. These inconsistencies are also reflected in the degraded fit to the data.

JCAP09(2026)080

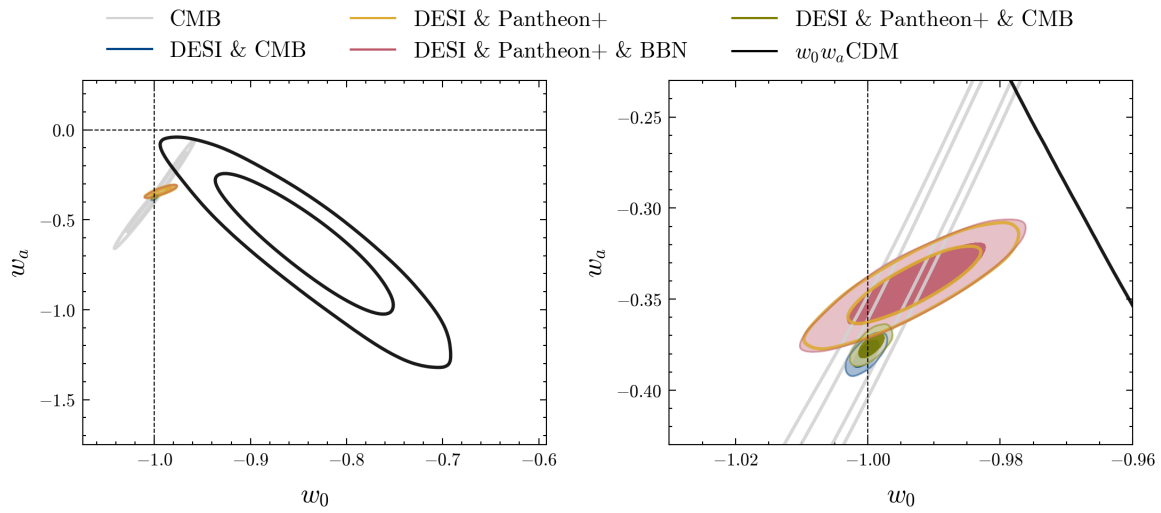


Figure 4. *Left:* derived constraints on the equation of state parameter $w(a = 1)$ and its derivative $w_a = -\frac{dw}{da}(a = 1)$ today for GREA. Note that the parametrization $w(a) = w_0 + w_a(1 - a)$ does not capture the full behavior of the equation of state in GREA (figure 1). These two parameters only capture the very low-z behavior, and we report them here for comparison with the standard w_0-w_a analysis. A negative slope $w_a \sim -0.3$ is quite a generic prediction from GREA, while its value today w_0, depends on the value of α, as illustrated in figure 1. *Right:* zoomed in version around the region favoured by GREA. The black contour shows the w_0w_aCDM constraints from the DESI DR2 & Pantheon+ & CMB (P-ACT) combination.

Data	$\Delta\chi^2$	$\chi^2_{\rm GREA}$	$\chi^2_{\Lambda\rm CDM}$	$\chi^2_{\Lambda\rm CDM+\Omega_k}$	$\chi^2_{w_0w_a}$
DESI & BBN	3.6	13.9	10.3	9.9	5.6
DESI & CMB	3.0	17.0	13.9	10.5	7.3
DESI & Pantheon+ & BBN	5.9	1422.1	1416.2	1414.4	1411.3
DESI & Pantheon+ & PR4	13.4	1433.5	1420.1	1416.0	1413.0
DESI & Pantheon+ & SH_0ES	5.8	1471.2	1465.3	1463.6	1460.5
DESI & Pantheon+ & PR4 & SH_0ES	0.4	1498.2	1497.8	1490.1	1490.4

Table 2. The goodness of fit for different models and dataset combinations, $\Delta\chi^2$, obtained with the minimizer iMinuit [101]. The second column shows $\Delta\chi^2 \equiv \chi^2_{\rm GREA} - \chi^2_{\Lambda\rm CDM}$. Note that CMB here refers to Planck PR4.

by subtle differences in preferred $\Omega_{\rm m,0}$, is a key reason why many late-time modifications to the expansion history struggle to resolve the "cosmic calibration" problem [16, 92, 100], especially when combining the Hubble diagrams probed by SNe Ia and BAO. We quantify the ability of GREA to ease the Hubble tension in section 5.3, where we compare the Gaussian tension with the SH_0ES measurement across all four models considered in this work, finding that GREA achieves a tension of $\sim 2.5\sigma$ with BBN calibration, at the cost of a degraded fit to the combined data.

JCAP09(2026)080

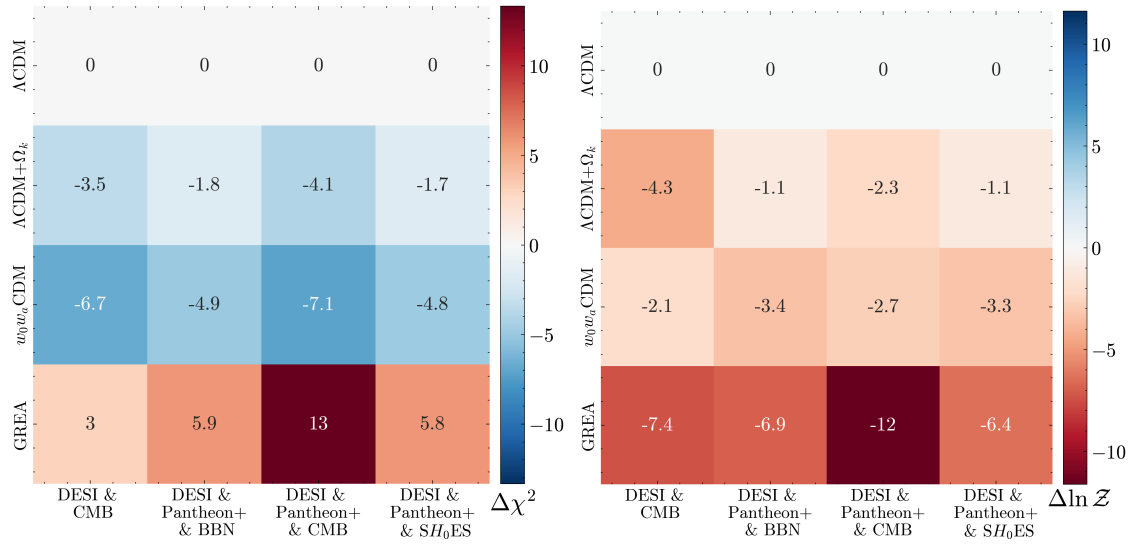


Figure 5. Visual representation of the goodness of fit compared to the ΛCDM model, for the different models and dataset combinations as shown in table 2: $\Delta\chi^2 \equiv \chi^2_{\rm i} - \chi^2_{\Lambda\rm CDM}$ (left), and $\Delta \ln \mathcal{Z} = \log \mathcal{Z}^{\rm i} - \log \mathcal{Z}^{\Lambda\rm CDM}$ values (right). The Bayesian evidence, $\mathcal{Z}$, is computed using POLYCHORD [88].

Finally, it is insightful to introduce an *effective* dark energy density $\rho^{\rm eff}_{\rm DE}$ as

$$\Omega_{\rm DE,0}\ f_{\rm DE}(z) \equiv \left(\frac{H(z)}{H(0)}\right)^2 - \Omega_{\rm m,0}(1+z)^3 - \Omega_{\rm r,0}(1+z)^4\,, \tag{5.1}$$

where $\Omega_{\rm DE,0} = \frac{8\pi G}{3H(0)^2}\rho^{\rm eff}_{\rm DE,0} \simeq (1-\Omega_{\rm m,0})$ and $f_{\rm DE}(z) = \rho^{\rm eff}_{\rm DE}(z)/\rho^{\rm eff}_{\rm DE,0}$ determines its redshift evolution, from which we can compute its *effective* equation of state, using

$$w(a) = -\frac{1}{3}\frac{{\rm d}\ln f_{\rm DE}}{{\rm d}\ln a} - 1 = -\frac{1}{3}\frac{{\rm d}\ln}{{\rm d}\ln a}\left[\frac{\sinh(2\tau)}{a^2}\right] - 1 \tag{5.2}$$

$$= -\frac{1}{3}\Big[2a\,\tau'(a)\coth[2\tau(a)] + 1\Big]\,. \tag{5.3}$$

The marginalized constraints on these two key quantities are depicted in figure 6 for the DESI & Pantheon+ & CMB data combination. These two quantities allow for a direct comparison of the best-fit GREA model with the data-driven (model-agnostic) reconstructions of the DE phenomenology, presented in [23, 24, 28]. The behaviour of $w(z)$ in GREA, particularly at low redshift, does not fully match the trends suggested by non-parametric, model-independent reconstructions. This mismatch is also reflected in the fit to the data, where the phenomenological w_0w_aCDM model—whose functional form closely follows the reconstructed $w(z)$—consistently outperforms both ΛCDM and GREA. While this discrepancy could have been anticipated from the allowed shape of $w(z)$ in GREA (figure 1) even before fitting, it is still valuable to confront the model with data, as this allows us to constrain its parameters and quantitatively assess its viability.

JCAP09(2026)080

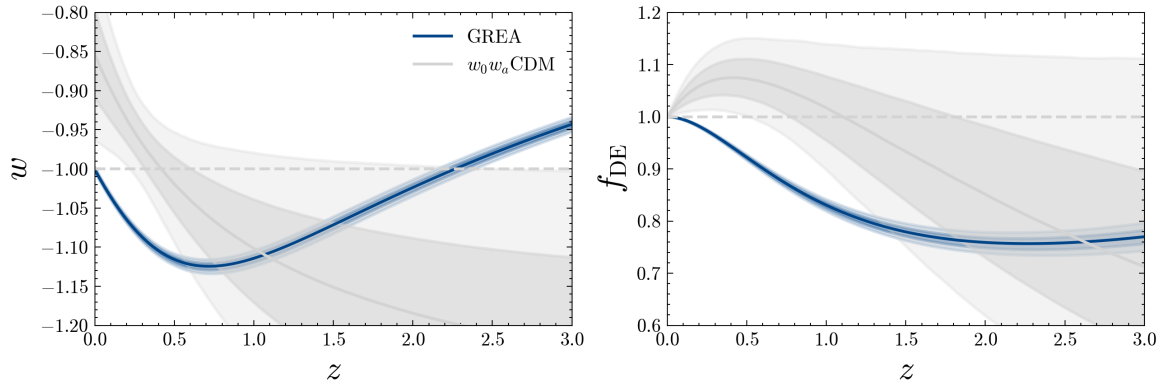


Figure 6. Constraints on the equation of state, w, and normalized energy density, $f_{\rm DE} = \rho_{\rm DE}/\rho_{\rm DE,0}$, from the DESI & Pantheon+ & CMB data combination in w_0w_aCDM (in gray; these are the predictive posterior obtained by propagating the w_0w_aCDM MCMC chains through $w(a) = w_0 + w_a(1-a)$) and GREA (in blue). The shaded bands represent the 68% and 95% confidence levels computed by drawing a large number of samples from the chains.

In figure 7, we display the best-fit predictions for the different models on top of BAO observables $D_V(z)/r_{\rm d}$ and $F_{\rm AP}(z) \equiv D_M/D_H$ normalized to their fiducial values.[6] The isotropic and anisotropic BAO distortion parameters at $0 < z < 1$ can help distinguish the best fit GREA and the w_0w_aCDM models (see figure 7).

When fitting the combined (DESI & Pantheon+ & CMB) data, the high-redshift evolution of the distance modulus is the same for both the best-fit GREA and w_0w_aCDM models describing current observations, except for very low redshift $z < 0.5$, where the increase in $H^{\rm GREA} > H^{\Lambda{\rm CDM}}$ leads to $D_L^{\rm GREA} < D_L^{\Lambda{\rm CDM}}$ (figure 8). Note that the uncalibrated Pantheon+ data (black circled datapoints) does not constrain H_0, nor M_B, but only their product. Thus, for a given H_0 there is freedom to choose the corresponding M_B that best fits the data. For simplicity, we normalize these measurements to the fiducial ΛCDM value. When calibrating distances with the cepheids-based ($\rm SH_0ES$) measurements (dashed lines in figure 8), as expected, the very low-z evolution is almost identical between the three models, and deviations only appear at intermediate redshift, where the w_0w_aCDM seems to fit the SN data better.

5.3 Implications for the Hubble tension

One of the most persistent tensions in modern cosmology is the ~ 4–5σ discrepancy between the value of the Hubble constant inferred from early-universe measurements [4] and the direct local measurement by the SH_0ES collaboration, $H_0^{\rm SH0ES} = 73.04 \pm 1.04$ km s^{-1} Mpc^{-1} [14]. As discussed in section 5.1, (uncalibrated) SNe Ia and BAO data only constrain the normalized expansion history $E(z) = H(z)/H_0$, and the degenerate combination H_0r_d. A calibration of the sound horizon — either through BBN or the CMB — is required to infer H_0 individually. Here we quantify the ability of GREA to ease this tension and compare it to ΛCDM,

[6] This corresponds to the baseline ΛCDM parameters used by the AbacusSummit suite of N-body simulations https://github.com/abacusorg/AbacusSummit/blob/main/Cosmologies/abacus_cosm000/CLASS.ini. For more details on the BAO measurements, see e.g. [102].

JCAP09(2026)080

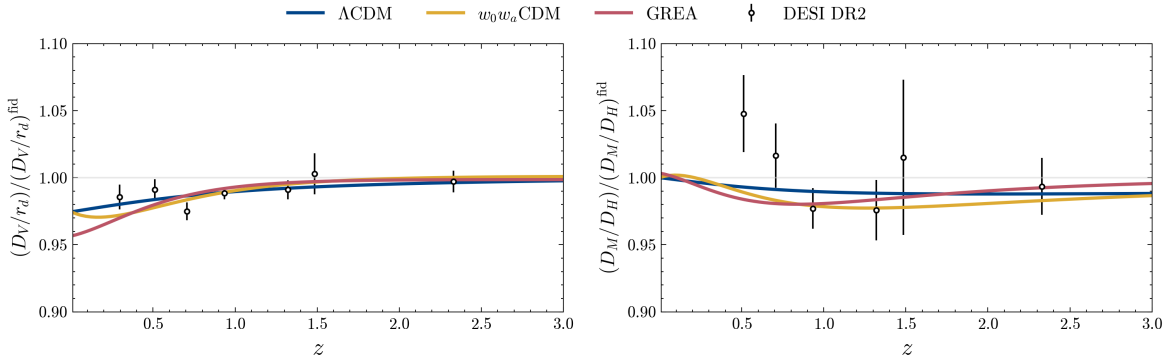


Figure 7. Evolution with redshift of the volume-averaged distance, D_V (left panel); and the anisotropic distortion measured with the comoving angular diameter distance signal, D_M (right panel, see details in section 3). Observational datasets are shown as open symbols. In each panel, the best fit model (BAO & SNeIa & CMB) for ΛCDMis shown by blue lines, GREA by red lines, and the w_0w_aCDMmodel by yellow lines. The largest differences between the GREA and w_0w_aCDM bestfit models are found at $z < 1$.

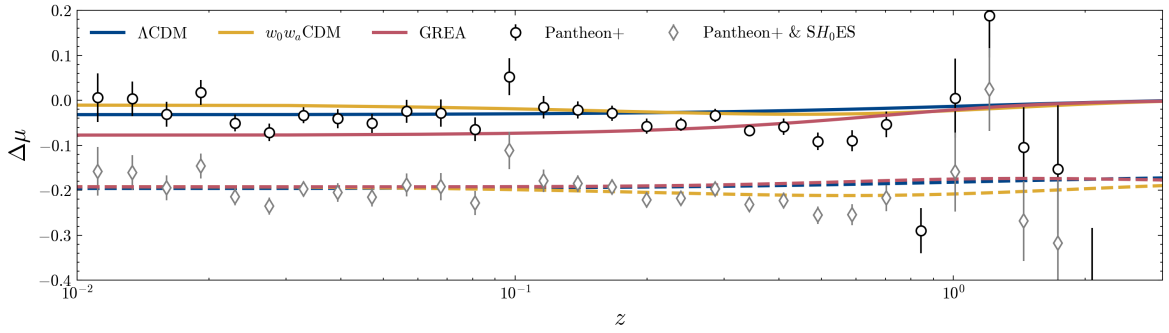


Figure 8. Evolution with redshift of the distance modulus residuals, $\Delta\mu = \mu - \mu^{\rm fid}$. The (uncalibrated) Pantheon+ are shown as open symbols, where as the SH_0ES -calibrated Pantheon+ measurements are shown as diamonds. The solid lines correspond to the best fit models to the full (DESI & Pantheon+& CMB) data combination. The dashed lines shows the corresponding bestfit predictions to the SH_0ES -calibrated (DESI & Pantheon+) measurements.

ΛCDM+Ω_k, and w_0w_aCDM. We use the Gaussian tension metric,

$$T = \frac{|H_0 - H_0^{\rm SH0ES}|}{\sqrt{\sigma_{H_0}^2 + \sigma_{\rm SH0ES}^2}}\,, \tag{5.4}$$

evaluated for each model and dataset combination, and report the results in figure 9.

The reason why GREA can raise H_0 relative to ΛCDM is rooted in its expansion history. As shown in figure 1, the GREA background features an enhanced $\dot{a} = aH(a)$ at low redshift compared to ΛCDM. With the BBN calibration, GREA achieves the lowest Hubble tension among the models considered, at the $\sim 2.5\sigma$ level, compared to ~ 3–4σ for ΛCDM. However, this improvement is not without cost: the higher H_0 implied by GREA, in combination with the large $\Omega_{\rm m,0}$ preferred by the SNe Ia and BAO data, drives an increase in the physical matter density $\omega_m = \Omega_{\rm m,0}h^2$, which degrades the fit to the CMB (table 2). Moreover, a

JCAP09(2026)080

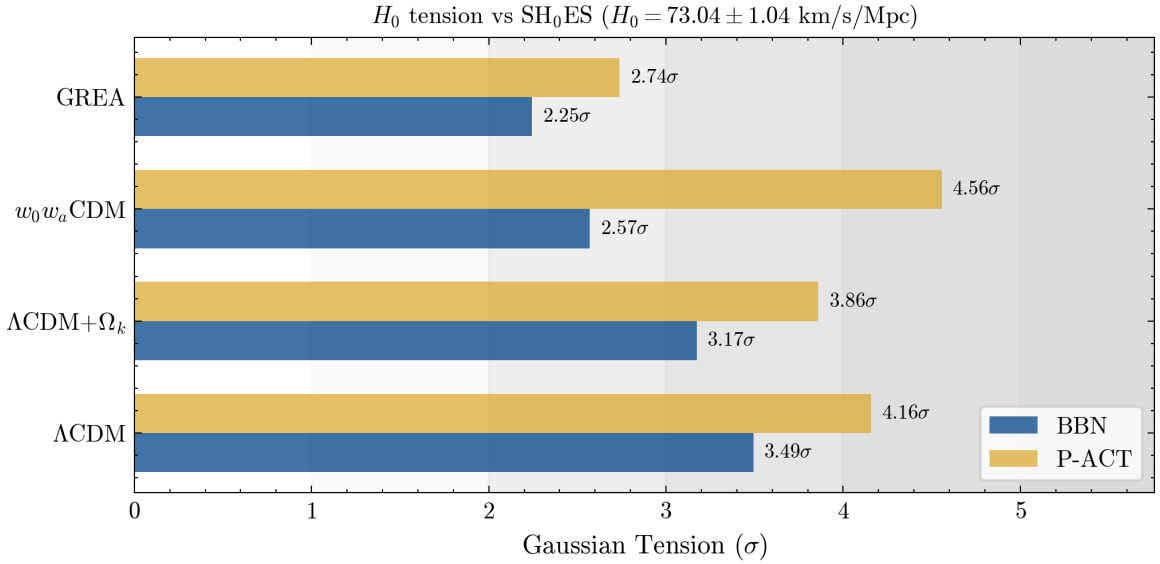


Figure 9. Gaussian tension with the SH_0ES estimation of $H_0 = 73.04 \pm 1.04$ km s^{-1} Mpc^{-1} [14], comparing the BBN (blue) and CMB-based (yellow) calibrations for the various models considered in this work. Due to its capacity to raise the value of H_0 (figure 1), consistently achieves the lowest tension among the models considered—reaching the $\sim 2.2\sigma$ ($\sim 2.7\sigma$) level with BBN (CMB) calibration, respectively—albeit with an overall degraded fit to the combined data (figure 5).

larger H_0—at fixed BAO angular scale—requires a smaller sound horizon, to match the observed peak positions. Since we work under the assumption of a (ΛCDM-like) early-time expansion history, the increase in H_0 naturally predicted by GREA cannot be compensated by a decrease in r_d. When the CMB calibration is used instead, the tight constraint on ω_m from the acoustic peaks suppresses this effect, and all models converge to similar tension levels of ~ 3–4σ. This illustrates the "cosmic calibration" tension [92]: late-time and early-time datasets impose conflicting requirements on H_0 and r_d that no simple modification of the late-time expansion history can simultaneously satisfy.

5.4 Further constraining GREA

In GREA, for scales of cosmological interest, the growth of density perturbations (in the linear regime) obeys [55]

$$a(\tau)\delta''(\tau) + a'(\tau)\delta'(\tau) = \frac{3}{2}\Omega_{\mathrm{m},0}\delta(\tau)\,, \tag{5.5}$$

where $\delta = \rho/\bar{\rho} - 1$ is matter density contrast and a prime denotes differentiation with respect to conformal time, τ. The modified growth of perturbations stems from the modified evolution of the scale factor, $a(\tau) \neq a^{\Lambda\mathrm{CDM}}$, encoded in the Hubble friction term above. It is convenient to rewrite the growth equation eq. (5.5) in terms of the growth factor $f \equiv \delta'/\delta = \frac{d\ln\delta}{d\ln a}$, giving

$$f'(a) + \left(f(a) + 2 + \frac{E'}{E}\right) f(a) = \frac{3}{2}\Omega_{\mathrm{m}}(a)\,, \tag{5.6}$$

JCAP09(2026)080

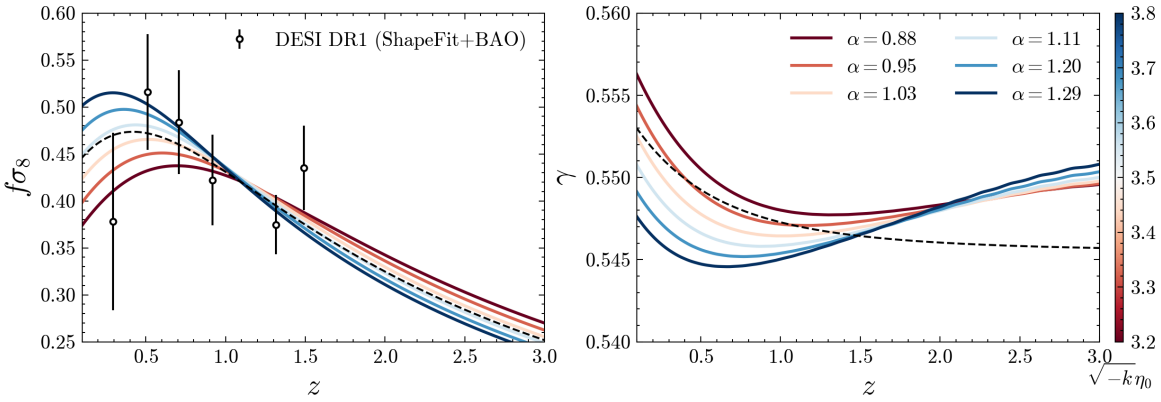


Figure 10. Growth of density perturbations as a function of redshift for the range of GREA predictions spanned by different values of α, illustrating the direct link between the single GREA parameter and the growth of cosmic structures. *Left:* evolution of the combination $f\sigma_8(z)$, probed by redshift-space distortions. *Right:* corresponding growth index $\gamma(z) \equiv \ln f(z)/\ln \Omega_m(z)$ evolution. The $f\sigma_8(z)$ measurements have been extracted from the DESI DR1 ShapeFit+BAO analysis [53]. These data points are shown for illustrative purposes only and have *not* been used in the parameter estimation presented in this work. The black dashed line on both panels corresponds to ΛCDM.

where $' \equiv d/d\ln a$, $\Omega_{\rm m}(a) = \Omega_{\rm m,0}\ a^{-3}E^{-2}$ and $E = H(z)/H_0$. We integrate eq. (5.6) with initial conditions deep in the matter dominated epoch, with $f(a_{\rm ini}) = 1$.[7] From an observational viewpoint, the relevant quantity is the combination [103]

$$f\sigma_8(a) \equiv f(a)\cdot\sigma_8(a) = \frac{\sigma_{8,0}}{\delta_0} f\delta = \frac{\sigma_{8,0}}{\delta_0}\delta', \tag{5.7}$$

where $\sigma_{8,0}$ is the amplitude of matter fluctuations, smoothed over scales of radius $R = 8h^{-1}$Mpc, and $\delta_0 = \delta(z=0)$. On the left panel of figure 10, we show the evolution of the growth rate $f\sigma_8(a)$ at late times for various GREA scenarios, along with the DESI DR1 measurements extracted from a ShapeFit+BAO analysis (table 11 in [53]). The present data constrain the background expansion history in GREA to be close to that of ΛCDM, with preferred values of $\alpha \sim 1.09$, seen in figure 3 and table 3. Therefore, the corresponding $f\sigma_8$ closely follows that of ΛCDM, as the growth history is fully determined by the expansion history for DE models inside GR. On the right panel, we display the evolution of the growth index $\gamma(z) \equiv \ln f(a)/\ln \Omega_m(a)$ [104–108]. Interestingly, while the present value of $\gamma \simeq 0.55$ is close to that of ΛCDM, at higher redshifts, $\gamma(z)$ has a very different behaviour, satisfying in particular $d\gamma/dz > 0$. This is in sharp contrast with the ΛCDM case, where $\gamma(z)$ is a monotonically decreasing function of redshift [109–111]. Forthcoming LSS measurements by DESI, in combination with Euclid and LSST, are expected to constrain γ and its derivative with high precision [112].

6 Conclusions

General Relativistic Entropic Acceleration (GREA) arises as a consequence of out of equilibrium phenomena associated with the growth of entropy of horizons. It is a consequence

[7] In an Einstein-DeSitter (EdS), or matter dominated universe, it is easy to show that $\delta(a) \propto a \Leftrightarrow f = 1$.

JCAP09(2026)080

of quantum gravity holography, which gives a correspondence between the dynamics in a volume of space and the degrees of freedom in the boundary of that space. The GREA theory offers a natural explanation for the universe's accelerated expansion without the need for a cosmological constant [49, 51, 54, 55]. The accelerated expansion in GREA is associated with the growth of entropy from cosmic and black hole horizons, making it a promising alternative to the cosmological constant, Λ. In addition, this theory introduces a single $\mathcal{O}(1)$ parameter α that encapsulates the effect of GREA as an evolving dark energy scenario, both at the background and perturbation level. GREA makes precise predictions for various cosmological observables that can be tested with increasingly accurate observations [55]. For our Universe, the causal horizon growth associated with the matter/energy content induces a growth in entropy of the horizon while driving a dynamical entropic acceleration, which is very different from that predicted by ΛCDM. Even in the absence of Λ, the entropic acceleration is enough to explain the dimming of distant SNe and the recent BAO data from DESI DR2 (figure 7). Moreover, GREA makes a specific prediction: that the size of our causal horizon today should be the same as the curvature scale ($\alpha \sim 1$).

In this work, we have used state-of-the-art BAO measurements by the DESI collaboration [22, 57, 60, 70, 102], together with other external datasets (section 3), to constrain the free parameters of GREA (section 4). GREA achieves a fit to observations comparable to the phenomenological ΛCDM model[8] (table 2 and figure 5). This is particularly encouraging as ΛCDM and GREA are not nested models. Despite the Bayesian evidence favouring the phenomenological ΛCDM model, the alternative GREA scenario remains compelling. We emphasize that usual model comparison metrics, such as $\Delta\chi^2$ and the Bayes ratio, should be interpreted with care for non-nested models, such as GREA and ΛCDM. We have reported the Bayes ratios assuming equal priors for the underlying models. Perhaps a more appropriate choice is to weight the alternative hypothesis according to their theoretical basis. This could potentially penalize ΛCDM and w_0w_aCDM with respect to GREA and change the odds in its favour. In the Bayesian framework, the preference for one model (M_1) over another (M_0) is usually assessed by computing the Bayes ratio, K, given by

$$K = \frac{\mathcal{Z}_1}{\mathcal{Z}_0} = \frac{\mathcal{P}(D|M_1)}{\mathcal{P}(D|M_0)} = \frac{\mathcal{P}(M_1|D)}{\mathcal{P}(M_0|D)} \frac{\Pi(M_0)}{\Pi(M_1)}\,, \tag{6.1}$$

where $\Pi(M_i)$ and $\mathcal{Z}_i = \mathcal{P}(D|M_i)$ are the prior probability and evidence for model M_i, respectively. The quantity $\mathcal{P}(M_i|D)$ is precisely what we want to estimate; that is, the probability of the model, given the observed data. Most of the times, we assume $\Pi(M_1) = \Pi(M_0) = 0.5$, as most DE models are purely phenomenological, and we cannot favour one over the other, purely on theoretical grounds. The ratio of Bayesian evidences should be weighted according to the reliability of the model priors. In particular, having values of Λ orders of magnitude below quantum gravity expectations should heavily penalize ΛCDMwhen compared against GREA. However, we have not taken this into account in our analysis and conclusions. We leave this analysis for a future publication.

Our analysis suggests that GREA can account for the data to some extent without invoking a fine-tuned (infinitesimally small and positive) cosmological constant. The best

[8] We note that χ^2 differences are reported relative to ΛCDM. The goodness of fit of ΛCDM has been assessed in previous works [53, 71].

JCAP09(2026)080

GREA model that fits the observational data point towards a *transient* phantom crossing at $z \leq 2$ (see figure 6). We note that we have worked under the assumption of a ΛCDM-expansion history at early times (in particular, at matter-radiation equality). It would be interesting to explore how alternative initial conditions, e.g., with an Early Dark Energy (EDE)−like component or modified physics at recombination, can alter the derived constraints. Moreover, we have assumed that the main effect of GREA comes from the *homogeneous* entropy growth of the cosmic horizon. If GREA arises also from the gravitational collapse of *inhomogeneous* structures that form the cosmic web [51], it may modify the late universe dynamics in a way that could be tested with future cosmological data. This analysis, however, requires non-linear N-body simulations which go beyond the state-of-the-art. We leave this for future work.

Additional observational data will be critical to further assess the viability of GREA. Data at $z < 1$, probing the growth of cosmic structures and the evolution of matter perturbations will be particularly interesting (figure 10). Forthcoming measurements from DESI and other stage-IV experiments will provide an opportunity to rigorously test the predictions of GREA across a wider range of cosmological observables.

Acknowledgments

R.C. would like to thank Vivian Poulin and Tristan L. Smith for insightful discussions. This work was supported by the high-performance computing cluster Seondeok at the Korea Astronomy and Space Science Institute. R.C. is funded by the Czech Ministry of Education, Youth and Sports (MEYS) and European Structural and Investment Funds (ESIF) under project number CZ.02.01.01/00/22_008/0004632. J.G-B acknowledges support from the Research Project PID2021-123012NB-C43 [MICINN-FEDER], and the Centro de Excelencia Severo Ochoa Program CEX2020-001007-S at Instituto de Física Teórica. B.V.G would like to acknowledge the support from the European Union (ERC StG, LSS BeyondAverage, 101075919) and the Comunidad de Madrid 2019-T1/TIC-12702 grant. V.G.P. acknowledges support from Comunidad de Madrid in Spain (Atracción de Talento Contract grants: 2019-T1/TIC-12702 and 2023-5A/TIC-28943) and the Ministerio de Ciencia e Innovación (MICINN, grant PID2021-122603NB-C21). This material is based upon work supported by the U.S. Department of Energy (DOE), Office of Science, Office of High-Energy Physics, under Contract No. DE-AC02-05CH11231, and by the National Energy Research Scientific Computing Center, a DOE Office of Science User Facility under the same contract. Additional support for DESI was provided by the U.S. National Science Foundation (NSF), Division of Astronomical Sciences under Contract No. AST-0950945 to the NSF's National Optical-Infrared Astronomy Research Laboratory; the Science and Technology Facilities Council of the United Kingdom; the Gordon and Betty Moore Foundation; the Heising-Simons Foundation; the French Alternative Energies and Atomic Energy Commission (CEA); the National Council of Humanities, Science and Technology of Mexico (CONAHCYT); the Ministry of Science, Innovation and Universities of Spain (MICIU/AEI/10.13039/501100011033), and by the DESI Member Institutions: https://www.desi.lbl.gov/collaborating-institutions. Any opinions, findings, and conclusions or recommendations expressed in this material are those of the author(s) and do not necessarily reflect the views of the U.S. National Science Foundation, the U.S. Department of Energy, or any of the listed funding agencies.

JCAP09(2026)080

Datasets	$\Omega_{m,0}$	$10^2\omega_b$	$H_0[\mathrm{km\,s^{-1}\,Mpc^{-1}}]$	α
DESI & Pantheon+	0.323 ± 0.012	–	–	$1.1067^{+0.0044}_{-0.0049}$
(Uncalibrated)	(0.316)	(–)	(–)	(1.092)
DESI & BBN	0.300 ± 0.011	2.23 ± 0.05	70.9 ± 1.5	1.105 ± 0.013
	(0.298)	(2.23)	(70.8)	(1.104)
DESI & Union3 & BBN	0.315 ± 0.010	2.23 ± 0.05	69.5 ± 1.3	1.094 ± 0.012
	(0.315)	(2.23)	(69.4)	(1.092)
DESI & DES-SN5YR & BBN	0.326 ± 0.008	2.23 ± 0.05	68.6 ± 1.2	1.088 ± 0.012
	(0.325)	(2.23)	(69.5)	(1.087)
DESI & Pantheon+ & BBN	0.317 ± 0.009	2.23 ± 0.05	69.4 ± 1.3	1.093 ± 0.012
	(0.316)	(2.23)	(69.4)	(1.093)
DESI & PR4	0.288 ± 0.004	2.217 ± 0.014	70.4 ± 0.5	1.0994 ± 0.0029
	(0.287)	(2.215)	(70.4)	(1.099)
DESI & P-ACT	0.287 ± 0.004	2.247 ± 0.011	70.4 ± 0.5	1.0962 ± 0.0023
	(0.287)	(2.247)	(70.4)	(1.096)
DESI & Pantheon+ & PR4	0.292 ± 0.004	2.216 ± 0.014	69.9 ± 0.5	1.0995 ± 0.0027
	(0.292)	(2.215)	(69.9)	(1.099)
DESI & Pantheon+ & P-ACT	0.291 ± 0.004	2.247 ± 0.011	69.9 ± 0.5	1.0961 ± 0.0024
	(0.291)	(2.246)	(69.8)	(1.096)
DESI & Pantheon+ & SH_0ES	0.317 ± 0.009	2.68 ± 0.14	72.9 ± 1.3	1.092 ± 0.012
	(0.316)	(2.646)	(72.8)	(1.093)
DESI & Pantheon+ & PR4 & SH_0ES	0.287 ± 0.004	2.218 ± 0.014	70.6 ± 0.5	1.0997 ± 0.0029
	(0.287)	(2.218)	(70.6)	(1.100)
DESI & Pantheon+ & P-ACT & SH_0ES	0.286 ± 0.004	2.248 ± 0.011	70.5 ± 0.5	1.0967 ± 0.0024
	(0.285)	(2.247)	(70.6)	(1.096)

Table 3. 68% credible intervals for the cosmological parameters in GREA, using various dataset combinations. We also report the *maximum a posteriori* (MAP) values in parentheses, obtained with the minimizer iMinuit [101].

The authors are honored to be permitted to conduct scientific research on I'oligam Du'ag (Kitt Peak), a mountain with particular significance to the Tohono O'odham Nation.

Data availability. Data from the plots in this paper will be made available on Zenodo (https://zenodo.org/records/22682067) as part of DESI's Data Management Plan.

A Parameter constraints

In table 3, we report the marginalized constraints on the cosmological parameters of GREA, for the various data combinations considered in this work.

B Comparison with DESI DR1

Throughout this work, we have used the BAO constraints from DESI DR2. We explore how the constrains have improved going from DR1 to DR2 in figure 11. DESI DR2 contains 6671 dark tiles, increasing by a factor of 2.4 the number of objects released in DR1 [71].

JCAP09(2026)080

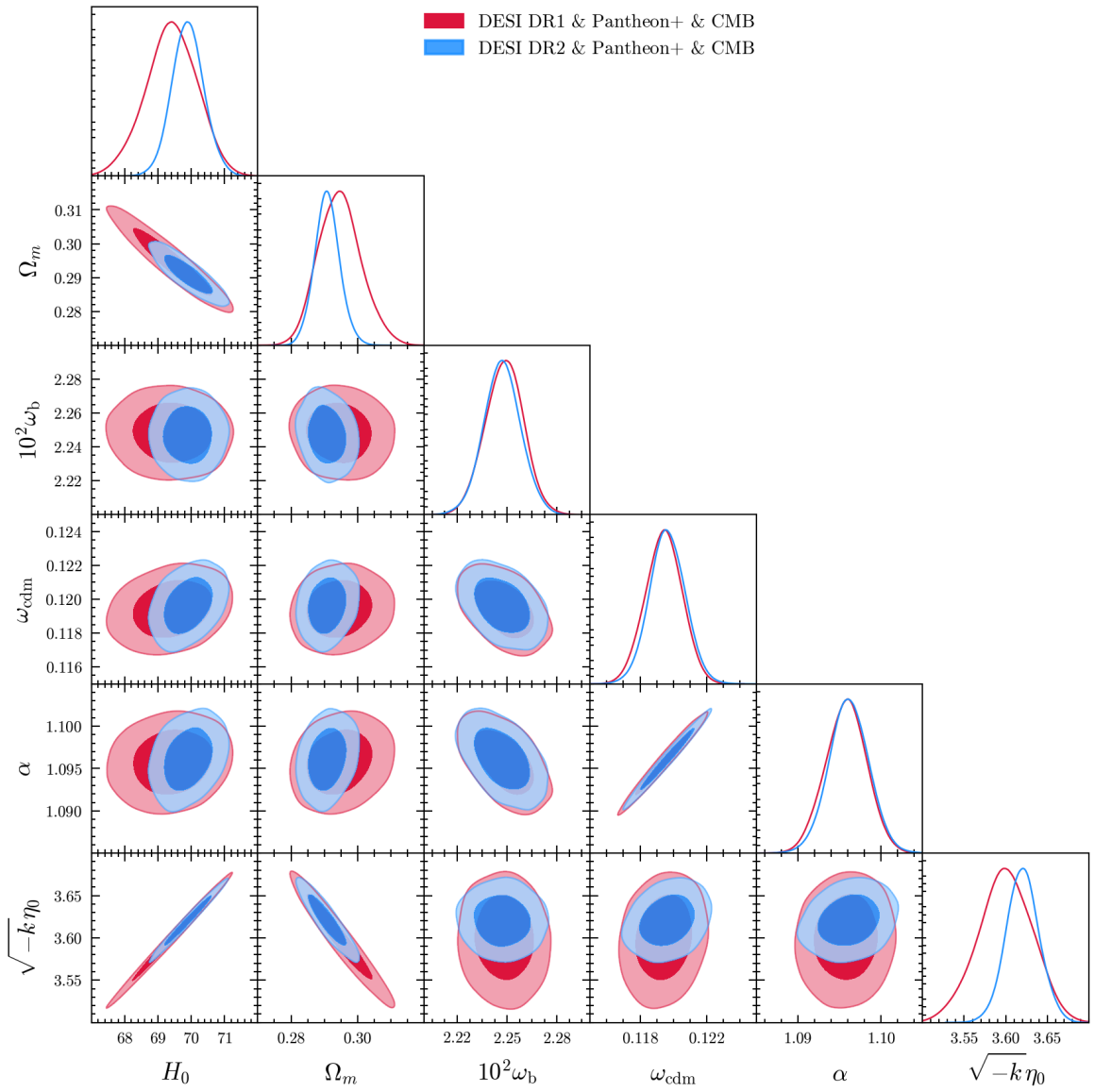


Figure 11. Similar to figure 2 but comparing the results using either DESI DR1 or DR2, combined with the Pantheon+ sample and the CMB data from P-ACT. The constraining power in the curvature scale parameter, $\sqrt{-k}\eta_0$, is improved by 60% when moving from DESI DR1 to DESI DR2, including also SNe Ia and CMB data.

We find that the constrains improved by a factor of ~ 2 when moving from DR1 to DR2. The central values stay within 1σ. The trends seen for the central values are similar to the results shown in figure 2 when removing the SN data from the DESI DR2 & Pantheon+ & CMB. In terms of the curvature scale parameter, $\sqrt{-k}\eta_0$, the constraints in DR2 are 60% tighter than in DR1.

JCAP09(2026)080

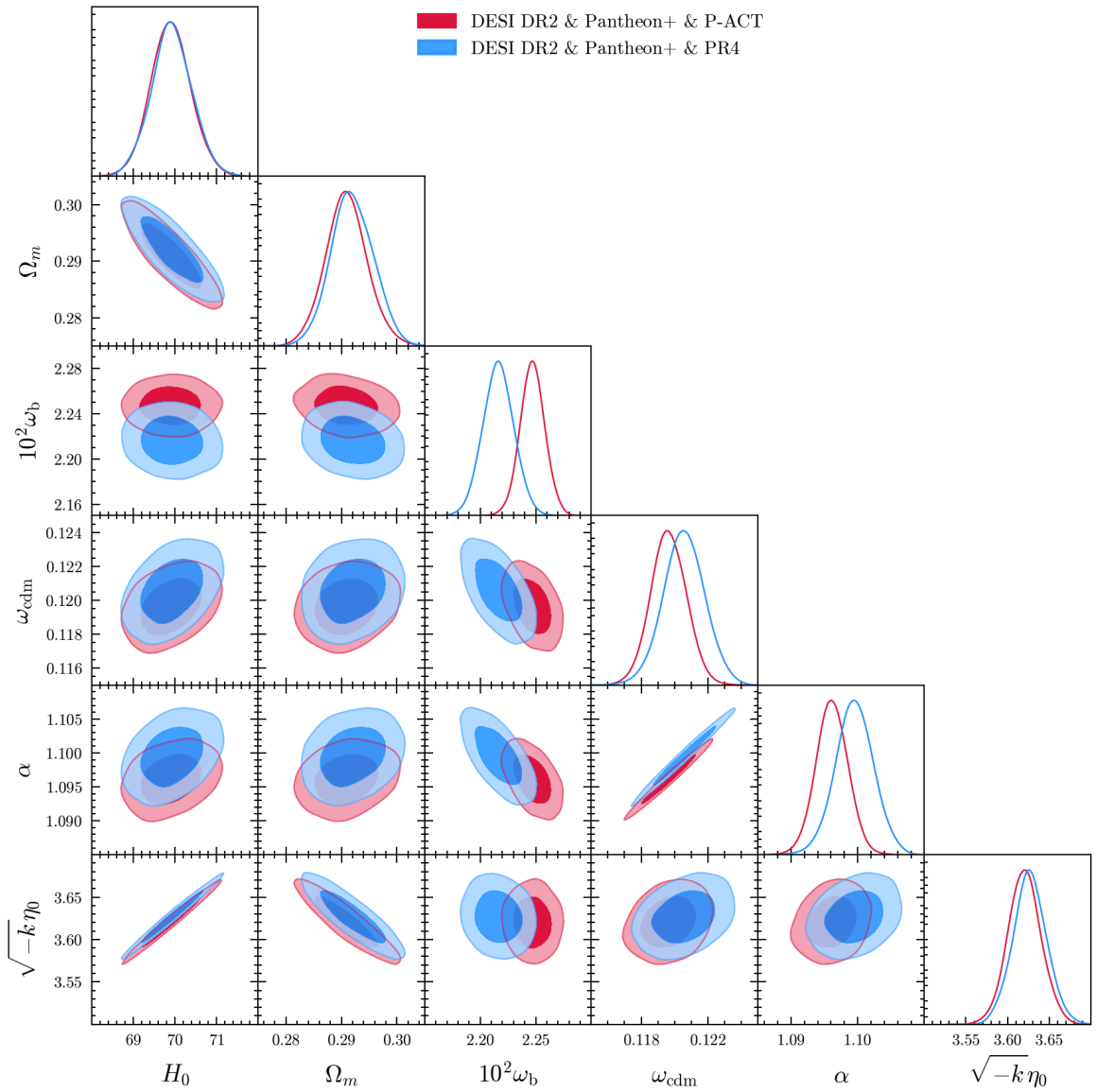


Figure 12. Comparison of the constraints obtained using the compressed CMB measurements of $(\theta_s, \omega_b, \omega_{bc})$ extracted from either Planck (CamSpec) PR4, or the Planck PR3+ACT (P-ACT) combination.

C CMB compression and comparison with CamSpec PR4

In this appendix, we compare the constraints obtained using the CamSpec CMB likelihood, based on the Planck PR4 maps, with those obtained from the Planck and ACT (P-ACT) combination [75, 76]. These results are shown infigure 12. The compressed CMB information from the Planck (PR4) chains can be found in appendix A of ref. [71]. Here, we provide the

JCAP09(2026)080

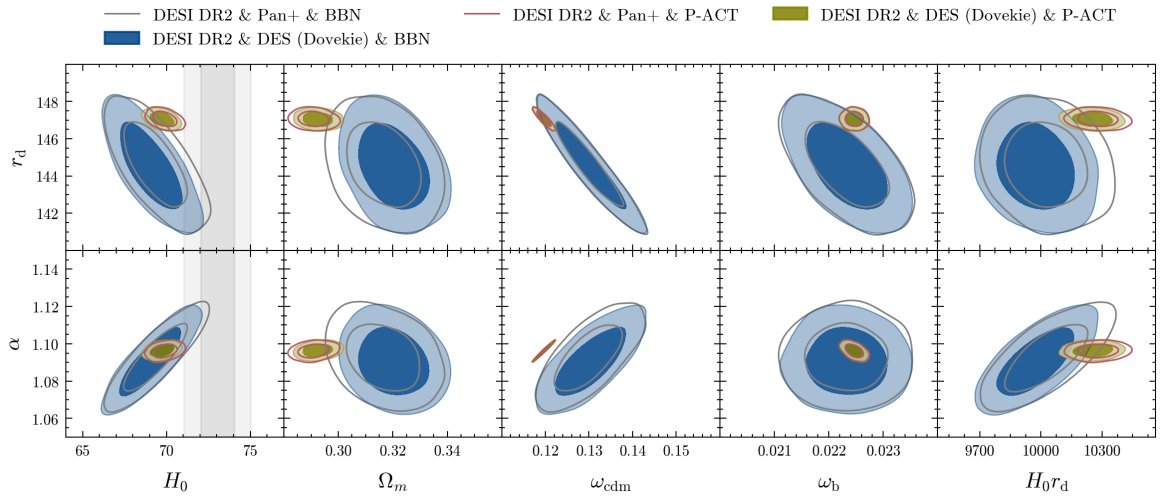


Figure 13. Marginalized constraints on GREA parameters using the DES-Dovekie SNe Ia compilation [113] (filled contours), compared against our baseline Pantheon+ results (unfilled contours). The posteriors are fully consistent and our conclusions remain unchanged.

equivalent from the P-ACT chains [75]. The data vector and covariance matrix are given by

$$\vec{\mathcal{D}} = \begin{pmatrix} 100\,\theta_s \\ \omega_{\rm b} \\ \omega_{\rm bc} \end{pmatrix} = \begin{pmatrix} 1.04165 \\ 0.0225046 \\ 0.141640 \end{pmatrix}, \tag{C.1}$$

$$\Sigma = \begin{pmatrix} 6.64717\times10^{-8} & 2.71701\times10^{-9} & -3.92400\times10^{-8} \\ 2.71701\times10^{-9} & 1.20267\times10^{-8} & -3.49601\times10^{-8} \\ -3.92400\times10^{-8} & -3.49601\times10^{-8} & 1.11695\times10^{-6} \end{pmatrix}, \tag{C.2}$$

from which we construct the likelihood $-2\ln\mathcal{L} = \chi^2$ in the usual way,

$$\chi^2 = \vec{r}^{\,T}\cdot\Sigma^{-1}\cdot\vec{r} \tag{C.3}$$

where $\vec{r}$ is the residual vector between the theoretical predictions and the data vector $\vec{\mathcal{D}}$.

D Impact of the DES Y5 Dovekie reanalysis

The DES-SN5YR photometric sample has recently been recalibrated in the DES-Dovekie reanalysis [113], which adopts an improved photometric calibration pipeline and reduces the preference for dynamical dark energy in the w_0w_aCDM parametrization. Here we assess whether this recalibration has any significant impact on the constraints derived for GREA.

We repeat the baseline analysis of section 5 replacing Pantheon+ with the DES-Dovekie likelihood, while keeping all other datasets and priors identical. The resulting posteriors are shown in figure 13, compared against our baseline Pantheon+ results. We find that the impact on the GREA parameters is minimal: the posteriors obtained with DES-Dovekie are fully consistent with the baseline, and the inferred value of α and the goodness of fit relative to ΛCDM are essentially unaffected by the recalibration. Our overall conclusions therefore remain unchanged.

JCAP09(2026)080

References

[1] V. Sahni and A.A. Starobinsky, *The case for a positive cosmological Λ term*, *Int. J. Mod. Phys. D* **9** (2000) 373 [astro-ph/9904398] [INSPIRE].

[2] Supernova Search Team collaboration, *Observational evidence from supernovae for an accelerating universe and a cosmological constant*, *Astron. J.* **116** (1998) 1009 [astro-ph/9805201] [INSPIRE].

[3] Supernova Cosmology Project collaboration, *Measurements of Ω and Λ from 42 high redshift supernovae*, *Astrophys. J.* **517** (1999) 565 [astro-ph/9812133] [INSPIRE].

[4] Planck collaboration, *Planck 2018 results. I. Overview and the cosmological legacy of Planck*, *Astron. Astrophys.* **641** (2020) A1 [arXiv:1807.06205] [INSPIRE].

[5] eBOSS collaboration, *Completed SDSS-IV extended Baryon Oscillation Spectroscopic Survey: cosmological implications from two decades of spectroscopic surveys at the Apache Point Observatory*, *Phys. Rev. D* **103** (2021) 083533 [arXiv:2007.08991] [INSPIRE].

[6] eBOSS collaboration, *The completed SDSS-IV extended Baryon Oscillation Spectroscopic Survey: cosmological implications from multitracer BAO analysis with galaxies and voids*, *Mon. Not. Roy. Astron. Soc.* **511** (2022) 5492 [arXiv:2110.03824] [INSPIRE].

[7] S. Weinberg, *The cosmological constant problem*, *Rev. Mod. Phys.* **61** (1989) 1 [INSPIRE].

[8] S.M. Carroll, *The cosmological constant*, *Living Rev. Rel.* **4** (2001) 1 [astro-ph/0004075] [INSPIRE].

[9] P. Bull et al., *Beyond ΛCDM: problems, solutions, and the road ahead*, *Phys. Dark Univ.* **12** (2016) 56 [arXiv:1512.05356] [INSPIRE].

[10] J.S. Bullock and M. Boylan-Kolchin, *Small-scale challenges to the ΛCDM paradigm*, *Ann. Rev. Astron. Astrophys.* **55** (2017) 343 [arXiv:1707.04256] [INSPIRE].

[11] L. Perivolaropoulos and F. Skara, *Challenges for ΛCDM: an update*, *New Astron. Rev.* **95** (2022) 101659 [arXiv:2105.05208] [INSPIRE].

[12] E. Abdalla et al., *Cosmology intertwined: a review of the particle physics, astrophysics, and cosmology associated with the cosmological tensions and anomalies*, *JHEAp* **34** (2022) 49 [arXiv:2203.06142] [INSPIRE].

[13] R. Calderón, A. Shafieloo, D.K. Hazra and W. Sohn, *On the consistency of ΛCDM with CMB measurements in light of the latest Planck, ACT and SPT data*, *JCAP* **08** (2023) 059 [arXiv:2302.14300] [INSPIRE].

[14] A.G. Riess et al., *A comprehensive measurement of the local value of the Hubble constant with 1 km s^{-1} Mpc^{-1} uncertainty from the Hubble Space Telescope and the SH0ES team*, *Astrophys. J. Lett.* **934** (2022) L7 [arXiv:2112.04510] [INSPIRE].

[15] E. Di Valentino et al., *In the realm of the Hubble tension — a review of solutions*, *Class. Quant. Grav.* **38** (2021) 153001 [arXiv:2103.01183] [INSPIRE].

[16] N. Schöneberg et al., *The H_0 olympics: A fair ranking of proposed models*, *Phys. Rept.* **984** (2022) 1 [arXiv:2107.10291] [INSPIRE].

[17] A.H. Wright et al., *KiDS-Legacy: cosmological constraints from cosmic shear with the complete Kilo-Degree Survey*, *Astron. Astrophys.* **703** (2025) A158 [arXiv:2503.19441] [INSPIRE].

[18] HSC collaboration, *Cosmology from cosmic shear power spectra with Subaru Hyper Suprime-Cam first-year data*, *Publ. Astron. Soc. Jap.* **71** (2019) 43 [arXiv:1809.09148] [INSPIRE].

JCAP09(2026)080

[19] KiDS collaboration, *KiDS-1000 cosmology: cosmic shear constraints and comparison between two point statistics*, *Astron. Astrophys.* **645** (2021) A104 [arXiv:2007.15633] [INSPIRE].

[20] DES collaboration, *Dark Energy Survey year 3 results: cosmological constraints from galaxy clustering and weak lensing*, *Phys. Rev. D* **105** (2022) 023520 [arXiv:2105.13549] [INSPIRE].

[21] E. Di Valentino et al., *Cosmology intertwined III: $f\sigma_8$ and S_8*, *Astropart. Phys.* **131** (2021) 102604 [arXiv:2008.11285] [INSPIRE].

[22] DESI collaboration, *DESI 2024 VI: cosmological constraints from the measurements of baryon acoustic oscillations*, *JCAP* **02** (2025) 021 [arXiv:2404.03002] [INSPIRE].

[23] DESI collaboration, *Extended dark energy analysis using DESI DR2 BAO measurements*, *Phys. Rev. D* **112** (2025) 083511 [arXiv:2503.14743] [INSPIRE].

[24] DESI collaboration, *DESI 2024: reconstructing dark energy using crossing statistics with DESI DR1 BAO data*, *JCAP* **10** (2024) 048 [arXiv:2405.04216] [INSPIRE].

[25] DESI collaboration, *DESI 2024 VII: cosmological constraints from the full-shape modeling of clustering measurements*, *JCAP* **07** (2025) 028 [arXiv:2411.12022] [INSPIRE].

[26] DESI collaboration, *DESI 2024: constraints on physics-focused aspects of dark energy using DESI DR1 BAO data*, *Phys. Rev. D* **111** (2025) 023532 [arXiv:2405.13588] [INSPIRE].

[27] M. Ishak et al., *Modified gravity constraints from the full shape modeling of clustering measurements from DESI 2024*, *JCAP* **09** (2025) 053 [arXiv:2411.12026] [INSPIRE].

[28] DESI collaboration, *Dynamical dark energy in light of the DESI DR2 baryonic acoustic oscillations measurements*, *Nature Astron.* **9** (2025) 1879 [*Erratum ibid.* **9** (2025) 1898] [arXiv:2504.06118] [INSPIRE].

[29] W. Elbers et al., *Negative neutrino masses as a mirage of dark energy*, *Phys. Rev. D* **111** (2025) 063534 [arXiv:2407.10965] [INSPIRE].

[30] W. Elbers et al., *Constraints on neutrino physics from DESI DR2 BAO and DR1 full shape*, *Phys. Rev. D* **112** (2025) 083513 [arXiv:2503.14744] [INSPIRE].

[31] X. Chen and A. Loeb, *Evolving dark energy or dark matter with an evolving equation-of-state?*, *JCAP* **07** (2025) 059 [arXiv:2505.02645] [INSPIRE].

[32] M. Braglia, X. Chen and A. Loeb, *Exotic dark matter and the DESI anomaly*, *JCAP* **11** (2025) 064 [arXiv:2507.13925] [INSPIRE].

[33] G.P. Lynch, L. Knox and J. Chluba, *DESI observations and the Hubble tension in light of modified recombination*, *Phys. Rev. D* **110** (2024) 083538 [arXiv:2406.10202] [INSPIRE].

[34] DESI collaboration, *Positive neutrino masses with DESI DR2 via matter conversion to dark energy*, *Phys. Rev. Lett.* **135** (2025) 081003 [arXiv:2504.20338] [INSPIRE].

[35] E. Chaussidon et al., *Early time solution as an alternative to the late time evolving dark energy with DESI DR2 BAO*, *Phys. Rev. D* **112** (2025) 063548 [arXiv:2503.24343] [INSPIRE].

[36] S.-F. Chen and M. Zaldarriaga, *It's all ok: curvature in light of BAO from DESI DR2*, *JCAP* **08** (2025) 014 [arXiv:2505.00659] [INSPIRE].

[37] S.H. Mirpoorian, K. Jedamzik and L. Pogosian, *Is dynamical dark energy necessary? DESI BAO and modified recombination*, *JCAP* **12** (2025) 050 [arXiv:2504.15274] [INSPIRE].

[38] N. Sailer, G.S. Farren, S. Ferraro and M. White, *Addressing tensions in ΛCDM cosmology by an increase in the optical depth to reionization*, *Phys. Rev. Lett.* **136** (2026) 081002 [arXiv:2504.16932] [INSPIRE].

JCAP09(2026)080

[39] A. Shafieloo, U. Alam, V. Sahni and A.A. Starobinsky, *Smoothing supernova data to reconstruct the expansion history of the universe and its age*, *Mon. Not. Roy. Astron. Soc.* **366** (2006) 1081 [astro-ph/0505329] [INSPIRE].

[40] T. Holsclaw et al., *Nonparametric reconstruction of the dark energy equation of state*, *Phys. Rev. D* **82** (2010) 103502 [arXiv:1009.5443] [INSPIRE].

[41] A. Shafieloo, A.G. Kim and E.V. Linder, *Gaussian process cosmography*, *Phys. Rev. D* **85** (2012) 123530 [arXiv:1204.2272] [INSPIRE].

[42] S. Nesseris and J. García-Bellido, *A new perspective on dark energy modeling via genetic algorithms*, *JCAP* **11** (2012) 033 [arXiv:1205.0364] [INSPIRE].

[43] R. Calderón et al., *Joint reconstructions of growth and expansion histories from stage-IV surveys with minimal assumptions: dark energy beyond* Λ, *Phys. Rev. D* **106** (2022) 083513 [arXiv:2206.13820] [INSPIRE].

[44] R. Calderón et al., *Joint reconstructions of growth and expansion histories from stage-IV surveys with minimal assumptions. II. Modified gravity and massive neutrinos*, *Phys. Rev. D* **108** (2023) 023504 [arXiv:2301.00640] [INSPIRE].

[45] M. Chevallier and D. Polarski, *Accelerating universes with scaling dark matter*, *Int. J. Mod. Phys. D* **10** (2001) 213 [gr-qc/0009008] [INSPIRE].

[46] E.V. Linder, *Exploring the expansion history of the universe*, *Phys. Rev. Lett.* **90** (2003) 091301 [astro-ph/0208512] [INSPIRE].

[47] R.R. Caldwell and E.V. Linder, *The limits of quintessence*, *Phys. Rev. Lett.* **95** (2005) 141301 [astro-ph/0505494] [INSPIRE].

[48] R. de Putter and E.V. Linder, *Calibrating dark energy*, *JCAP* **10** (2008) 042 [arXiv:0808.0189] [INSPIRE].

[49] J. García-Bellido and L. Espinosa-Portales, *Cosmic acceleration from first principles*, *Phys. Dark Univ.* **34** (2021) 100892 [arXiv:2106.16014] [INSPIRE].

[50] L. Espinosa-Portalés and J. García-Bellido, *Covariant formulation of non-equilibrium thermodynamics in general relativity*, *Phys. Dark Univ.* **34** (2021) 100893 [arXiv:2106.16012] [INSPIRE].

[51] J. García-Bellido, *Cosmic entropic acceleration from supermassive black hole growth*, *Phys. Dark Univ.* **44** (2024) 101491 [arXiv:2306.10593] [INSPIRE].

[52] DES collaboration, *The Dark Energy Survey: cosmology results with* ~ 1500 *new high-redshift type Ia supernovae using the full 5 yr data set*, *Astrophys. J. Lett.* **973** (2024) L14 [arXiv:2401.02929] [INSPIRE].

[53] DESI collaboration, *DESI 2024 V: full-shape galaxy clustering from galaxies and quasars*, *JCAP* **09** (2025) 008 [*Erratum ibid.* **02** (2026) E02] [arXiv:2411.12021] [INSPIRE].

[54] R. Arjona, L. Espinosa-Portales, J. García-Bellido and S. Nesseris, *A GREAT model comparison against the cosmological constant*, *Phys. Dark Univ.* **36** (2022) 101029 [arXiv:2111.13083] [INSPIRE].

[55] J. García-Bellido, *Dark energy predictions from GREA: background and linear perturbation theory*, *Phys. Dark Univ.* **45** (2024) 101533 [arXiv:2405.02895] [INSPIRE].

[56] DESI collaboration, *DESI DR2: data release 2 of the Dark Energy Spectroscopic Instrument*, in preparation (2026).

[57] DESI collaboration, *DESI 2024 III: baryon acoustic oscillations from galaxies and quasars*, *JCAP* **04** (2025) 012 [arXiv:2404.03000] [INSPIRE].

[58] DESI collaboration, *The DESI experiment, a whitepaper for Snowmass 2013*, arXiv:1308.0847 [INSPIRE].

[59] DESI collaboration, *The DESI experiment part II: instrument design*, arXiv:1611.00037 [INSPIRE].

[60] DESI collaboration, *Overview of the instrumentation for the Dark Energy Spectroscopic Instrument*, *Astron. J.* **164** (2022) 207 [arXiv:2205.10939] [INSPIRE].

[61] DESI collaboration, *The robotic multiobject focal plane system of the Dark Energy Spectroscopic Instrument (DESI)*, *Astron. J.* **165** (2023) 9 [arXiv:2205.09014] [INSPIRE].

[62] DESI collaboration, *The optical corrector for the Dark Energy Spectroscopic Instrument*, *Astron. J.* **168** (2024) 95 [arXiv:2306.06310] [INSPIRE].

[63] DESI collaboration, *The spectroscopic data processing pipeline for the Dark Energy Spectroscopic Instrument*, *Astron. J.* **165** (2023) 144 [arXiv:2209.14482] [INSPIRE].

[64] DESI collaboration, *Survey operations for the Dark Energy Spectroscopic Instrument*, *Astron. J.* **166** (2023) 259 [arXiv:2306.06309] [INSPIRE].

[65] C. Poppett et al., *Overview of the fiber system for the Dark Energy Spectroscopic Instrument*, *Astron. J.* **168** (2024) 245.

[66] DESI collaboration, *Data release 1 of the Dark Energy Spectroscopic Instrument*, *Astron. J.* **171** (2026) 285 [arXiv:2503.14745] [INSPIRE].

[67] DESI collaboration, *The DESI experiment part I: science, targeting, and survey design*, arXiv:1611.00036 [INSPIRE].

[68] DESI collaboration, *Validation of the scientific program for the Dark Energy Spectroscopic Instrument*, *Astron. J.* **167** (2024) 62 [arXiv:2306.06307] [INSPIRE].

[69] DESI collaboration, *The early data release of the Dark Energy Spectroscopic Instrument*, *Astron. J.* **168** (2024) 58 [arXiv:2306.06308] [INSPIRE].

[70] DESI collaboration, *DESI 2024 IV: baryon acoustic oscillations from the Lyman α forest*, *JCAP* **01** (2025) 124 [arXiv:2404.03001] [INSPIRE].

[71] DESI collaboration, *DESI DR2 results. II. Measurements of baryon acoustic oscillations and cosmological constraints*, *Phys. Rev. D* **112** (2025) 083515 [arXiv:2503.14738] [INSPIRE].

[72] A. Aizpuru, R. Arjona and S. Nesseris, *Machine learning improved fits of the sound horizon at the baryon drag epoch*, *Phys. Rev. D* **104** (2021) 043521 [arXiv:2106.00428] [INSPIRE].

[73] D. Brout et al., *The Pantheon+ analysis: cosmological constraints*, *Astrophys. J.* **938** (2022) 110 [arXiv:2202.04077] [INSPIRE].

[74] D. Rubin et al., *Union through UNITY: cosmology with 2,000 SNe using a unified Bayesian framework*, *Astrophys. J.* **986** (2025) 231 [arXiv:2311.12098] [INSPIRE].

[75] Atacama Cosmology Telescope collaboration, *The Atacama Cosmology Telescope: DR6 power spectra, likelihoods and ΛCDM parameters*, *JCAP* **11** (2025) 062 [arXiv:2503.14452] [INSPIRE].

[76] Atacama Cosmology Telescope collaboration, *The Atacama Cosmology Telescope: DR6 constraints on extended cosmological models*, *JCAP* **11** (2025) 063 [arXiv:2503.14454] [INSPIRE].

JCAP09(2026)080

[77] J. Carron, M. Mirmelstein and A. Lewis, *CMB lensing from Planck PR4 maps*, *JCAP* **09** (2022) 039 [arXiv:2206.07773] [INSPIRE].

[78] ACT collaboration, *The Atacama Cosmology Telescope: DR6 gravitational lensing map and cosmological parameters*, *Astrophys. J.* **962** (2024) 113 [arXiv:2304.05203] [INSPIRE].

[79] ACT collaboration, *The Atacama Cosmology Telescope: a measurement of the DR6 CMB lensing power spectrum and its implications for structure growth*, *Astrophys. J.* **962** (2024) 112 [arXiv:2304.05202] [INSPIRE].

[80] N. Schöneberg, *The 2024 BBN baryon abundance update*, *JCAP* **06** (2024) 006 [arXiv:2401.15054] [INSPIRE].

[81] A. Lewis and S. Bridle, *Cosmological parameters from CMB and other data: a Monte Carlo approach*, *Phys. Rev. D* **66** (2002) 103511 [astro-ph/0205436] [INSPIRE].

[82] A. Lewis, *Efficient sampling of fast and slow cosmological parameters*, *Phys. Rev. D* **87** (2013) 103529 [arXiv:1304.4473] [INSPIRE].

[83] J. Torrado and A. Lewis, *Cobaya: code for Bayesian analysis of hierarchical physical models*, *JCAP* **05** (2021) 057 [arXiv:2005.05290] [INSPIRE].

[84] A. Gelman and D.B. Rubin, *Inference from iterative simulation using multiple sequences*, *Statist. Sci.* **7** (1992) 457 [INSPIRE].

[85] A. Lewis, *GetDist: a Python package for analysing Monte Carlo samples*, *JCAP* **08** (2025) 025 [arXiv:1910.13970] [INSPIRE].

[86] J. Pan, D. Huterer, F. Andrade-Oliveira and C. Avestruz, *Compressed baryon acoustic oscillation analysis is robust to modified-gravity models*, *JCAP* **06** (2024) 051 [arXiv:2312.05177] [INSPIRE].

[87] W.J. Handley, M.P. Hobson and A.N. Lasenby, *PolyChord: nested sampling for cosmology*, *Mon. Not. Roy. Astron. Soc.* **450** (2015) L61 [arXiv:1502.01856] [INSPIRE].

[88] W.J. Handley, M.P. Hobson and A.N. Lasenby, *polychord: next-generation nested sampling*, *Mon. Not. Roy. Astron. Soc.* **453** (2015) 4385 [arXiv:1506.00171] [INSPIRE].

[89] S. Nesseris and J. Garcia-Bellido, *Is the Jeffreys' scale a reliable tool for Bayesian model comparison in cosmology?*, *JCAP* **08** (2013) 036 [arXiv:1210.7652] [INSPIRE].

[90] H. Koo, R.E. Keeley, A. Shafieloo and B. L'Huillier, *Bayesian vs frequentist: comparing Bayesian model selection with a frequentist approach using the iterative smoothing method*, *JCAP* **03** (2022) 047 [arXiv:2110.10977] [INSPIRE].

[91] R.E. Keeley and A. Shafieloo, *On the distribution of Bayesian evidence*, *Mon. Not. Roy. Astron. Soc.* **515** (2022) 293 [arXiv:2111.04231] [INSPIRE].

[92] V. Poulin, T.L. Smith, R. Calderón and T. Simon, *Implications of the cosmic calibration tension beyond H_0 and the synergy between early- and late-time new physics*, *Phys. Rev. D* **111** (2025) 083552 [arXiv:2407.18292] [INSPIRE].

[93] D. Pedrotti et al., *Multidimensionality of the Hubble tension: the roles of Ω_m and ω_c*, *Phys. Rev. D* **111** (2025) 023506 [arXiv:2408.04530] [INSPIRE].

[94] M. Chu and L. Knox, *Testing cosmological models and understanding cosmological parameter determinations with metaparameters*, *Astrophys. J.* **620** (2005) 1 [astro-ph/0407198] [INSPIRE].

[95] P. Motloch, *Testing consistency of $\Omega_b h^2$ in the Planck data*, *Phys. Rev. D* **101** (2020) 123509 [arXiv:2004.11351] [INSPIRE].

JCAP09(2026)080

[96] I. Wasserman, *On the degeneracy inherent in observational determination of the dark energy equation of state*, *Phys. Rev. D* **66** (2002) 123511 [astro-ph/0203137] [INSPIRE].

[97] M. Kunz, *The dark degeneracy: on the number and nature of dark components*, *Phys. Rev. D* **80** (2009) 123001 [astro-ph/0702615] [INSPIRE].

[98] A. Shafieloo and E.V. Linder, *Cosmographic degeneracy*, *Phys. Rev. D* **84** (2011) 063519 [arXiv:1107.1033] [INSPIRE].

[99] R. von Marttens et al., *Dark degeneracy I: dynamical or interacting dark energy?*, *Phys. Dark Univ.* **28** (2020) 100490 [arXiv:1911.02618] [INSPIRE].

[100] R.E. Keeley and A. Shafieloo, *Ruling out new physics at low redshift as a solution to the H_0 tension*, *Phys. Rev. Lett.* **131** (2023) 111002 [arXiv:2206.08440] [INSPIRE].

[101] H. Dembinski et al., *scikit-hep/iminuit*, *Zenodo* (2020).

[102] DESI collaboration, *DESI 2024 II: sample definitions, characteristics, and two-point clustering statistics*, *JCAP* **07** (2025) 017 [arXiv:2411.12020] [INSPIRE].

[103] Y.-S. Song and W.J. Percival, *Reconstructing the history of structure formation using redshift distortions*, *JCAP* **10** (2009) 004 [arXiv:0807.0810] [INSPIRE].

[104] P.J.E. Peebles, *The peculiar velocity field in the local supercluster*, *Astrophys. J.* **205** (1976) 318.

[105] O. Lahav, P.B. Lilje, J.R. Primack and M.J. Rees, *Dynamical effects of the cosmological constant*, *Mon. Not. Roy. Astron. Soc.* **251** (1991) 128.

[106] L.-M. Wang and P.J. Steinhardt, *Cluster abundance constraints on quintessence models*, *Astrophys. J.* **508** (1998) 483 [astro-ph/9804015] [INSPIRE].

[107] E.V. Linder, *Cosmic growth history and expansion history*, *Phys. Rev. D* **72** (2005) 043529 [astro-ph/0507263] [INSPIRE].

[108] D. Polarski and R. Gannouji, *On the growth of linear perturbations*, *Phys. Lett. B* **660** (2008) 439 [arXiv:0710.1510] [INSPIRE].

[109] D. Polarski, A.A. Starobinsky and H. Giacomini, *When is the growth index constant?*, *JCAP* **12** (2016) 037 [arXiv:1610.00363] [INSPIRE].

[110] R. Calderon et al., *Global properties of the growth index of matter inhomogeneities in the universe*, *Phys. Rev. D* **100** (2019) 083503 [arXiv:1908.00117] [INSPIRE].

[111] R. Calderon et al., *Global properties of the growth index: mathematical aspects and physical relevance*, *Phys. Rev. D* **101** (2020) 103501 [arXiv:1912.06958] [INSPIRE].

[112] L. Amendola et al., *Cosmology and fundamental physics with the Euclid satellite*, *Living Rev. Rel.* **21** (2018) 2 [arXiv:1606.00180] [INSPIRE].

[113] DES collaboration, *The Dark Energy Survey supernova program: a reanalysis of cosmology results and evidence for evolving dark energy with an updated type Ia supernova calibration*, *Mon. Not. Roy. Astron. Soc.* **548** (2026) stag632 [arXiv:2511.07517] [INSPIRE].

JCAP09(2026)080

Author List

R. Calderon[a,*], J. García-Bellido[b,*], B. Vos-Ginés[c,ai], V. Gonzalez-Perez[c], A. Shafieloo[d,e], J. Aguilar[f], S. Ahlen[g], D. Bianchi[h,i], D. Brooks[j], T. Claybaugh[f], A. de la Macorra[k], J.E. Forero-Romero[l,m], E. Gaztañaga[n,o,p], S. Gontcho A Gontcho[f,q], G. Gutierrez[r], K. Honscheid[s,t,u], C. Howlett[v], M. Ishak[w], R. Joyce[x], R. Kehoe[y], T. Kisner[f], A. Kremin[f], O. Lahav[j], A. Lambert[f], M. Landriau[f], M. Manera[z,aa], R. Miquel[ab,aa], F. Prada[ac], I. Pérez-Ràfols[ad], E. Sanchez[ae], D. Schlegel[f], M. Schubnell[af,ag], J. Silber[f], D. Sprayberry[x], G. Tarlé[ag], B.A. Weaver[x], H. Zou[ah]

[a] *CEICO, Institute of Physics of the Czech Academy of Sciences, Na Slovance 1999/2, 182 21, Prague, Czech Republic*
[b] *Instituto de Física Teórica (IFT) UAM/CSIC, Universidad Autónoma de Madrid, Cantoblanco, E-28049, Madrid, Spain*
[c] *Centro de Investigación Avanzada en Física Fundamental (CIAFF), Facultad de Ciencias, Universidad Autónoma de Madrid, ES-28049 Madrid, Spain*
[d] *Korea Astronomy and Space Science Institute, 776, Daedeokdae-ro, Yuseong-gu, Daejeon 34055, Republic of Korea*
[e] *University of Science and Technology, 217 Gajeong-ro, Yuseong-gu, Daejeon 34113, Republic of Korea*
[f] *Lawrence Berkeley National Laboratory, 1 Cyclotron Road, Berkeley, CA 94720, U.S.A.*
[g] *Department of Physics, Boston University, 590 Commonwealth Avenue, Boston, MA 02215 U.S.A.*
[h] *Dipartimento di Fisica "Aldo Pontremoli", Università degli Studi di Milano, Via Celoria 16, I-20133 Milano, Italy*
[i] *INAF-Osservatorio Astronomico di Brera, Via Brera 28, 20122 Milano, Italy*
[j] *Department of Physics & Astronomy, University College London, Gower Street, London, WC1E 6BT, U.K.*
[k] *Instituto de Física, Universidad Nacional Autónoma de México, Circuito de la Investigación Científica, Ciudad Universitaria, Cd. de México C. P. 04510, Mexico*
[l] *Departamento de Física, Universidad de los Andes, Cra. 1 No. 18A-10, Edificio Ip, CP 111711, Bogotá, Colombia*
[m] *Observatorio Astronómico, Universidad de los Andes, Cra. 1 No. 18A-10, Edificio H, CP 111711 Bogotá, Colombia*
[n] *Institut d'Estudis Espacials de Catalunya (IEEC), c/ Esteve Terradas 1, Edifici RDIT, Campus PMT-UPC, 08860 Castelldefels, Spain*
[o] *Institute of Cosmology and Gravitation, University of Portsmouth, Dennis Sciama Building, Portsmouth, PO1 3FX, U.K.*
[p] *Institute of Space Sciences, ICE-CSIC, Campus UAB, Carrer de Can Magrans s/n, 08913 Bellaterra, Barcelona, Spain*
[q] *University of Virginia, Department of Astronomy, Charlottesville, VA 22904, U.S.A.*
[r] *Fermi National Accelerator Laboratory, PO Box 500, Batavia, IL 60510, U.S.A.*
[s] *Center for Cosmology and AstroParticle Physics, The Ohio State University, 191 West Woodruff Avenue, Columbus, OH 43210, U.S.A.*
[t] *Department of Physics, The Ohio State University, 191 West Woodruff Avenue, Columbus, OH 43210, U.S.A.*
[u] *The Ohio State University, Columbus, 43210 OH, U.S.A.*
[v] *School of Mathematics and Physics, University of Queensland, Brisbane, QLD 4072, Australia*
[w] *Department of Physics, The University of Texas at Dallas, 800 W. Campbell Rd., Richardson, TX 75080, U.S.A.*
[x] *NSF NOIRLab, 950 N. Cherry Ave., Tucson, AZ 85719, U.S.A.*
[y] *Department of Physics, Southern Methodist University, 3215 Daniel Avenue, Dallas, TX 75275, U.S.A.*
[z] *Departament de Física, Serra Húnter, Universitat Autònoma de Barcelona, 08193 Bellaterra (Barcelona), Spain*

JCAP09(2026)080

[aa] *Institut de Física d'Altes Energies (IFAE), The Barcelona Institute of Science and Technology, Edifici Cn, Campus UAB, 08193, Bellaterra (Barcelona), Spain*
[ab] *Institució Catalana de Recerca i Estudis Avançats, Passeig de Lluís Companys, 23, 08010 Barcelona, Spain*
[ac] *Instituto de Astrofísica de Andalucía (CSIC), Glorieta de la Astronomía, s/n, E-18008 Granada, Spain*
[ad] *Departament de Física, EEBE, Universitat Politècnica de Catalunya, c/Eduard Maristany 10, 08930 Barcelona, Spain*
[ae] *CIEMAT, Avenida Complutense 40, E-28040 Madrid, Spain*
[af] *Department of Physics, University of Michigan, 450 Church Street, Ann Arbor, MI 48109, U.S.A.*
[ag] *University of Michigan, 500 S. State Street, Ann Arbor, MI 48109, U.S.A.*
[ah] *National Astronomical Observatories, Chinese Academy of Sciences, A20 Datun Road, Chaoyang District, Beijing, 100101, P. R. China*
[ai] *Fakultät für Physik, Universität Bielefeld, Postfach 100131, 33501 Bielefeld, Germany*

[*] *Corresponding author*

JCAP09(2026)080